INSTITUTE OF PHYSICS PUBLISHING REPORTS ON PROGRESS IN PHYSICS

Rep. Prog. Phys. **68** (2005) 1811–1859 doi:10.1088/0034-4885/68/8/R03

Synchrotron facilities and the study of the Earth's deep interior

Thomas S Duffy

Department of Geosciences, Princeton University, Princeton, NJ 08544, USA

Received 19 April 2005
Published 5 July 2005
Online at stacks.iop.org/RoPP/68/1811

Abstract

The combination of synchrotron x-ray facilities with high-pressure methods provides new experimental tools for addressing geophysical problems relevant to understanding the interior of the Earth and other planets. Among the important geophysical questions related to the Earth's silicate mantle are the origin of seismic discontinuities in the upper mantle, the rheological properties of mantle minerals and their influence on dynamic flow in the Earth, and the nature of the core–mantle boundary region. In the case of the Earth's core, key questions are centred on the identity of the light elements of the core and their effect on energetics and thermodynamic properties, the melting curve of iron and its alloys and the origin of seismic anisotropy in the inner core.

Both new and established high-pressure synchrotron methods applied to the diamond anvil cell and large-volume apparatus are surveyed. Advances in synchrotron capabilities have been accompanied by new innovations in high-pressure technology. X-ray diffraction techniques are mature but continued improvements are leading to expanded pressure–temperature coverage and better ability to recover crystallographic details. Diffraction and absorption studies of the properties of liquids of silicate and iron alloy composition have expanded in response to new capabilities. Recently, methods for inelastic scattering and nuclear resonance probes have been developed at high pressures and these provide constraints on vibrational, electronic and magnetic properties, which were previously unattainable.

(Some figures in this article are in colour only in the electronic version)

Contents

1. Introduction

The geological activity that manifests itself so dramatically at the Earth's surface ultimately originates from the processes in the deep interior. Plate tectonics provides a coherent framework for describing the behaviour of the tectonic plates that cover the Earth's surface. However, the driving forces of plate tectonics remain poorly understood. Progress requires understanding the physical and chemical state of the planet's interior as well as its formation and evolution.

The solar system provides us with a range of planetary systems that are even more imperfectly understood than the Earth. As one example of the diversity of planetary styles, the Earth is the only planet on which plate tectonics is known to operate, but the reasons for its apparent absence on other planets are unclear. In addition planetary interiors provide natural laboratories for investigating the physical and chemical behaviour of materials under extreme conditions of pressure and temperature.

Understanding planetary structure and evolution requires a detailed knowledge of the properties of geological materials under conditions of deep planetary interiors. Experiments under such extreme conditions are challenging, however, and many fundamental properties remain poorly constrained or are inferred only through uncertain extrapolations from lower pressure–temperature (P–T) states.

In recent years, synchrotron-based techniques have played an ever-increasing role in the experimental effort to understand geological materials at high pressures and temperatures. Over the last decade, the development of new third-generation synchrotrons augmented by improvements in x-ray optics and detectors has led to dramatic advances in material property measurements at high pressures. The availability of synchrotron-based tools has also driven the development of new high-pressure designs. Differential stress in the sample, for example, rather than being a hindrance, is now being exploited for new experimental measurements. Established techniques, such as x-ray diffraction, are being used at higher pressures and temperatures with increased precision and accuracy of measurement. New techniques in high-pressure x-ray spectroscopy and scattering have greatly advanced capabilities for studying thermodynamic, elastic and electronic properties.

Section 2 of this review discusses the geophysical and geological constraints on the Earth's interior, emphasizing problems of recent interest. In section 3 developments in high-pressure and synchrotron tools for the Earth's interior research are surveyed. In sections 4 and 5, applications of recent synchrotron-based studies to the selected problems of the mantle and core are presented. In section 6, some speculations regarding future developments are noted.

2. An overview of the Earth's deep interior

Knowledge of deep planetary interiors is derived from a multi-disciplinary effort involving geophysical observations (e.g. seismology), geochemical analysis of rocks and the minerals derived directly or indirectly from the deep Earth, numerical simulations of convective flow of material under Earth conditions and the study (using both experiment and theory) of the physical and chemical properties of the Earth materials at high pressures and temperatures. Here an overview of recent progress from geophysical, geochemical and geodynamics research is given and some key issues of relevance for high-pressure synchrotron studies are highlighted.

2.1. Seismic structure of the Earth

The most direct information about the interior structure of the Earth comes from analysis of seismic waves generated by large earthquakes around the world. From globally averaged or

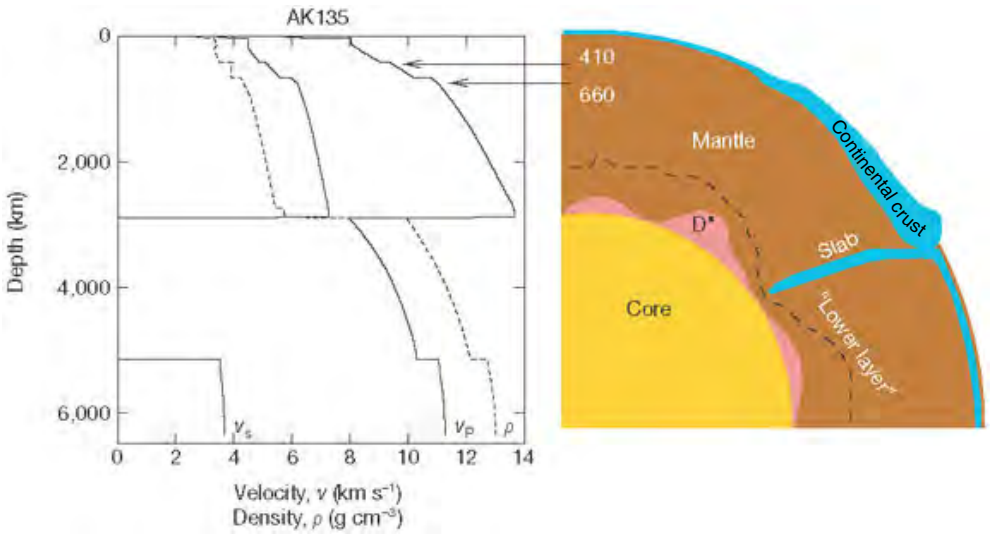

Figure 1. (Left) Globally averaged variation of compressional velocity (V_P), shear velocity (V_S) and density (ρ) with depth from Earth model AK135 [1]. (Right) Schematic illustration of major features of the Earth's interior. From [20].

regional profiles of compressional velocity, shear velocity and density with depth [1], the basic structure of the Earth's interior is revealed (figure 1). The Earth's crust varies in thickness from 0 to 70 km and is on an average 35 km thick under the continents and 7 km thick under the oceans. Below the crust lies the mantle. The mantle is divided into the upper mantle and lower mantle by an abrupt increase in seismic velocity at 660 km depth. Another major seismic discontinuity occurs near 410 km depth. In between the two discontinuities is a region of anomalously steep seismic gradient known as the transition zone. The uppermost mantle, above 410 km depth, is characterized by strong regional variations in velocity and, in certain regions, by a seismic low-velocity zone.

The lithosphere is the rigid, thermal boundary layer that overlies the hotter, ductile mantle undergoing convective motion. Under the oceanic regions, the lithosphere can reach a thickness up to ∼100–130 km, while the lithosphere under the continents can be up to 250 km thick. The oceanic lithosphere consists of SiO_2-rich basaltic oceanic crust underlaid by SiO_2-poor and MgO-rich peridotite layers. The oceanic lithosphere returns to the mantle at subduction zones, which are regions of abundant volcanic and seismic activity (figure 1).

In general, the lower mantle, extending from 660 km depth to the core mantle boundary near 2900 km depth, exhibits a smoother variation of seismic velocity with depth. The layer that lies 200–300 km above the core–mantle boundary, known for historical reasons as D″, is one of the most obscure yet important parts of the mantle, having extreme lateral heterogeneity and anomalous properties [2]. A global seismic discontinuity has been reported to exist at the top of the layer [3, 4]. Local regions of very low seismic velocities (ultra-low velocity zones) are interpreted in terms of partial melting at the base of the mantle and/or chemical reactions between the mantle and the core [5]. D″ may be the source region for volcanic hot spots such as Hawaii [6]. It may also be important as the final resting place for the subducting slabs. As discussed later, recent synchrotron experiments at pressures in excess of 100 GPa have identified a new structural phase transition that may finally provide a coherent explanation for some of the features of this region.

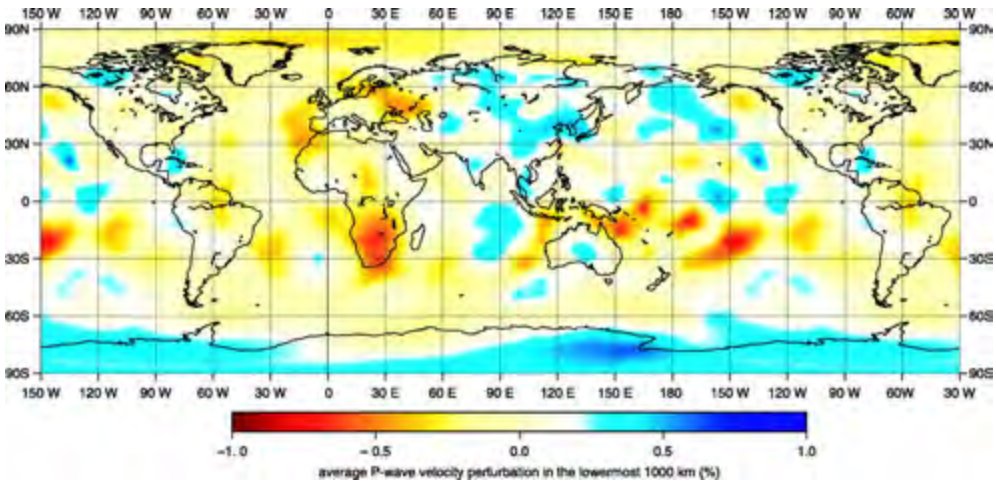

Figure 2. Vertical average of finite frequency tomographic results over the bottom 1000 km of the Earth's mantle. Red regions exhibit relative compressional velocity perturbations ($\delta V_P/V_P$) that are slower than average and blue regions are faster than average. From [9].

Over the last 20 years, seismologists have made major strides in constraining the three-dimensional seismic structure in the mantle, using seismic tomography [7] (figure 2). Tomographic studies are able to resolve the velocity variations associated with subducting lithospheric plates and thereby image their interaction with the 660 km seismic discontinuity. While a range of behaviour is observed at different subduction zones, evidence of slab penetration through the 660 km discontinuity at many subduction zones provides strong support for a mantle-wide circulation system [8]. More recently, tomographic studies have examined the nature of rising plumes of hot material (hot spots) [9], and the scale and degree of heterogeneity in the deep mantle [10]. The velocity variations imaged by tomography can mostly be ascribed to the effects of temperature [11, 12] but chemistry and phase may also be important, especially in certain regions such as the subcontinental lithosphere and the deepest mantle. Synchrotron studies play a major role in constraining the thermoelastic properties of minerals needed to interpret the tomographic images.

The Earth's core accounts for about one-third of the planet's mass. Based on a number of lines of evidence including shock compression data and cosmochemical considerations, the core is inferred to be predominantly iron, but experimental studies show that the core must also contain ∼10% lighter element by mass (see [13] for a review of core properties). Candidate light elements for the core include S, O, Si, C and H. The core itself is divided into a liquid outer core and a small, solid inner core with a 1228 km radius. The Earth's core plays an important role in the energetics and dynamics of the planet and provides the source for the Earth's magnetic field. The Earth's inner core is believed to be growing over time as the Earth cools. Information on the history of the geomagnetic field and hence the evolution of the core is contained in surface rocks which record the paleomagnetic field direction and intensity of the time of their formation. A comparison of seismologically determined densities of the inner core with those expected for iron under the relevant P–T conditions suggests that the inner core is also likely to contain some light element but perhaps only half as much as the outer core [14]. The selective rejection of light elements upon crystallization at the inner core boundary provides a source of compositional buoyancy that is likely to be an important contributor to the driving forces for convection in the fluid outer core [15]. Also, there is

seismological evidence that the inner core has some degree of layering. The inner core is elastically anisotropic with seismic waves travelling about 3% faster in the direction of the rotation axis compared with the waves travelling in the equatorial plane.

While seismology provides the strongest constraints on the nature of the Earth's interior with depth, other geophysical measurements also place observational constraints on the interior. Experimental studies at high pressures and temperatures are necessary for the interpretation of many of these measurements. Bulk planetary properties such as the mass, mean density and moment of inertia provide the zeroth order constraints. Other information comes from variations in the gravity field, topography, tidal response, rotation rate, intrinsic magnetic field and surface heat flow [16]. With the exception of the Moon, seismic data are unavailable for other planets and satellites in the solar system. Nevertheless, considerable insight into the behaviour of the interior and properties of bodies across the solar system can still be deduced by remote observations together with reasonable inferences derived through appropriate analogies with the Earth's behaviour.

2.2. Geochemical evidence on the makeup of the Earth's mantle

The chemistry of the Earth's mantle is inferred from direct petrological data supplemented by constraints on the bulk chemical composition of the Earth. Direct samples of the uppermost mantle (including mantle peridotites and xenoliths trapped in kimberlites or basalts) provide constraints on the chemistry of the upper 200 km or so of the Earth's mantle, although how representative these samples are of the region as a whole remains an open question. Less direct (but perhaps more representative) constraints on the mantle come from the study of the detailed composition of basalts that are derived from the upper mantle by the process of partial melting at mid-ocean ridges. Mineral inclusions in diamond [17] provide rare samples of the deep mantle and these have been inferred to originate from the depths to the transition zone or even the lower mantle. Interpretation of all these samples is augmented by constraints on the Earth's bulk chemistry [18] largely derived from the estimation of the solar system chemical abundances (from measurements of the solar photosphere and primitive meteorites) together with models for the accretion, differentiation and evolution of the Earth.

The dominant picture that has emerged from such analyses specifies that the uppermost mantle is composed of an Fe- and Mg-rich rock type known as peridotite that has been depleted in low-melting point components by the process of basalt formation at mid-ocean ridges. Determining whether the composition of deeper regions matches that of the uppermost mantle is one of the major ongoing directions of high-pressure synchrotron-based research. The average upper mantle is dominated by five oxide components: SiO_2, MgO, FeO, Al_2O_3 and CaO. A peridotite (or pyrolite) composition can then be specified in terms of four primary end-member minerals: olivine ($(Mg,Fe)_2SiO_4$), orthopyroxene ($(Mg,Fe)SiO_3$), clinopyroxene ($CaMgSi_2O_6$) and pyrope-rich garnet ($(Mg,Fe,Ca)_3Al_2Si_3O_{12}$). Olivine is the dominant upper mantle mineral component in this model (about 60% by volume). Experimental studies have revealed that each of the four end-members undergoes a series of phase transformations under compression (figure 3). For realistic mantle compositions, the picture is complicated by interactions and mutual solubility among the phases. For example, at upper mantle conditions, pyroxenes dissolve into the garnet structure producing an Al-deficient majorite garnet [19, 20].

The connection between this geochemical model and the geophysical observations discussed above comes from the fact that at expected temperatures of the mantle, phase

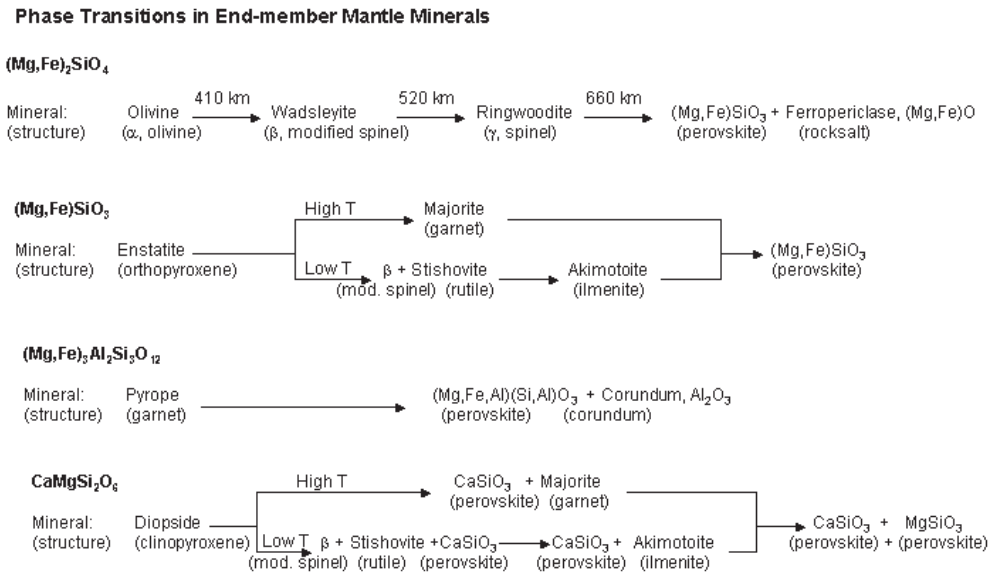

Figure 3. A simplified chart showing phase transformations in end-member upper minerals. The approximate mantle depth corresponding to olivine transitions is indicated. For pyroxenes, representative high temperature (normal mantle) and low temperature (subducting slab) paths are shown. All end-members transform to perovskite or perovskite-bearing assemblages at pressures of ∼25 GPa (650–700 km depth).

transformations in olivine occur at pressures corresponding roughly to those at depths of 410 and 660 km, the major seismic discontinuities of the upper mantle. On this basis, it is expected that the bulk chemical composition inferred from near-surface rocks may extend across the entire upper mantle, and perhaps through the Earth's mantle as a whole. However, more stringent tests of the model require consideration of the exact depth of the discontinuities as well as the amplitude and width of the discontinuities and how these quantities vary regionally. Mineralogical models with somewhat lower olivine contents (∼40%) provide a better fit to the seismic data at 410 km [21, 22]. The presence of phase transitions also does not rule out the existence of chemical changes.

A notable finding from the studies of the four end-member mineral compositions at high pressures is that, ultimately, all, transform to assemblages that are dominated by perovskite-structured phases. The perovskite-forming reactions produce atomic configurations with silicon in octahedral rather than tetrahedral coordination by oxygen. Such transformations occur at depths corresponding to the transition zone and in the vicinity of the 660 km discontinuity. Thus, from a mineralogical viewpoint, the 660 km discontinuity also plays a central role in the Earth's mantle because of this fundamental change in the structural unit that serves as the backbone of the various mineral phases.

While the bulk of the mantle may be represented by the phases found in peridotites or pyrolite compositions, on consideration of a wider range of compositions including plausible compositions in subducted oceanic crusts (some of which are geochemically altered), subducted sediments and other environments, the number of potential mineral phases becomes large (e.g. [23]). Over the last two decades, a major effort of synchrotron-based mineral physics research has been to characterize the stability, phase transitions and equations of state of the minerals (and appropriate analogue compositions) that may form from the variety of plausible mantle chemical compositions.

2.3. Mantle circulation

Mantle convection is the process by which the Earth slowly cools through the transport of interior heat to the surface. At subduction zones, the slowly moving (approximately a few centimetres per year) lithospheric plates plunge back into the mantle as part of this global mantle circulation system. The major focus of current research is to understand the nature of subduction and mantle convection. In particular, a key question is the extent to which the mantle is compositionally uniform or whether large-scale heterogeneities exist which have survived long-term convective mixing processes. A related issue is the role that the major seismic discontinuities play in the overall mantle circulation scheme [24]. Some geochemical evidence obtained from analysis of the distribution of trace elements and radiogenic isotopes in different rock types favours the existence of long-lived chemically isolated reservoirs, associated perhaps with major seismic discontinuities [10]. However, evidence from seismic tomography suggests that many subducting lithospheric slabs penetrate through the 660 km discontinuity, although other slabs are impeded or deflected by the boundary [8]. Computer models simulating mantle flow also generally favour the whole mantle rather than layered convection [10, 25]. Mantle convection occurs through solid-state flow driven by density contrasts. Therefore, in order to characterize the driving forces for mantle flow, it is necessary to understand all the contributions to density variations including chemical, thermal and structural effects as a function of P and T for candidate phases. Similarly, the interpretation of velocity anomalies imaged by seismic tomography in terms of variations in temperature, composition and phase also requires a detailed understanding of structural and thermodynamic properties of mantle minerals and their variation with pressure and temperature. It is also necessary to understand the flow laws which govern solid-state deformation of minerals in different regimes of the Earth's mantle [26–28].

There is intriguing seismic evidence of chemical heterogeneity in the deep mantle [29,30]. For example, observed anti-correlations between relative variations in shear wave velocity and density or shear and bulk wave velocities in the deep lower mantle are inconsistent with the explanation solely in terms of thermal effects and imply that there must also be significant lateral compositional variations [31, 32]. Based on this and other lines of reasoning, it has been suggested that the bottom third of the mantle may be geochemically distinct, and more heterogeneous, although no global sharp discontinuity in seismic velocity has been detected there [29].

2.4. Subduction zones

Subduction, the process by which the lithospheric plates are recycled into the mantle, provides a mechanism to inject chemical heterogeneity into the deep Earth (figure 4). The subducting slabs consist of a layer of basalt-composition crust overlying chemically depleted mantle. There are several fundamental questions associated with subduction zones and their role in Earth processes.

Subduction zones are associated with intermediate (100–300 km depth) and deep (300–680 km depth) earthquakes. The existence of such earthquakes is puzzling as the temperatures in the subducting slabs should be so high that ductile flow rather than brittle failure should be the dominant deformation mechanism under these conditions. A number of hypotheses have been proposed to explain the existence of deep seismicity. One possibility is that olivine, in the cold interior portion of the slab, continues to exist metastably far below the depth of the 410 km discontinuity. A sudden transformation to one of its high-pressure polymorphs might trigger an earthquake-generating instability. Other possibilities include

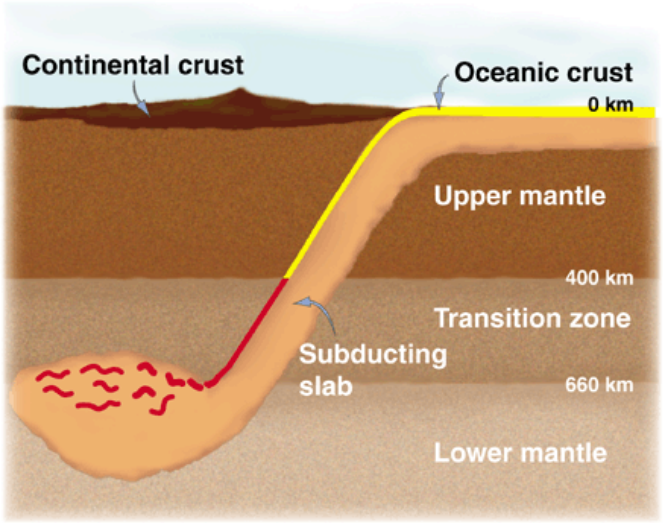

Figure 4. Schematic illustration of possible behaviour of the subducting lithosphere showing ponding near the 660 km discontinuity. Yellow and red regions at the top of the slab are subducting oceanic crust. Remainder (tan region) is lithospheric mantle. From [352].

metamorphic dehydration reactions in hydrous minerals or plastic instabilities. A detailed understanding of deformation behaviour under differential stress conditions, and the kinetics and mechanisms of phase transformations in mantle minerals including hydrous minerals, is needed to understand the deep earthquake process.

Another key issue related to subduction zones is their role in recycling volatiles (H_2O, CO_2, etc) into the mantle. Hydrogen remains one of the most poorly constrained compositional variables in the mantle. During subduction, slabs undergo a series of metamorphic reactions that release water into the overlying mantle and promote melting. How much water can yet be retained to be transported into the deep mantle is a subject of ongoing investigation. Owing to its large size, the mantle has the potential to store vast quantities of volatiles even if they are present in small amounts in individual mineral phases. Hydrated mineral systems include nominally anhydrous minerals that incorporate variable amounts of OH as defects, hydrous silicates of metamorphic environments and a class of dense hydrous magnesium silicates—each of these groups has members that could potentially harbour water deep into the upper and also the lower mantle [33]. The presence of hydrogen can affect properties such as elasticity [34], strength [35,36] and melting temperature. Small amounts of hydroxyl can cause large changes in the effective viscosity of rock, and hence can influence the rate and pattern of mantle flow. There is increasing geophysical evidence for hydrated regions in the Earth's interior [37–39].

2.5. Role of synchrotron-based high-pressure research

Pressures in the deep Earth are determined from the density distribution with depth (figure 1). The pressure at the base of the upper mantle (660 km) corresponds to about 24 GPa, whereas that at the core–mantle boundary is 135 GPa. The inner-core boundary is at a pressure of nearly 330 GPa and the pressure at the centre of the Earth is 363 GPa. Temperatures are considerably more uncertain, and the plausible temperature range of interest for the mantle is shown in figure 5. Near-surface constraints on temperatures come from a variety of lines

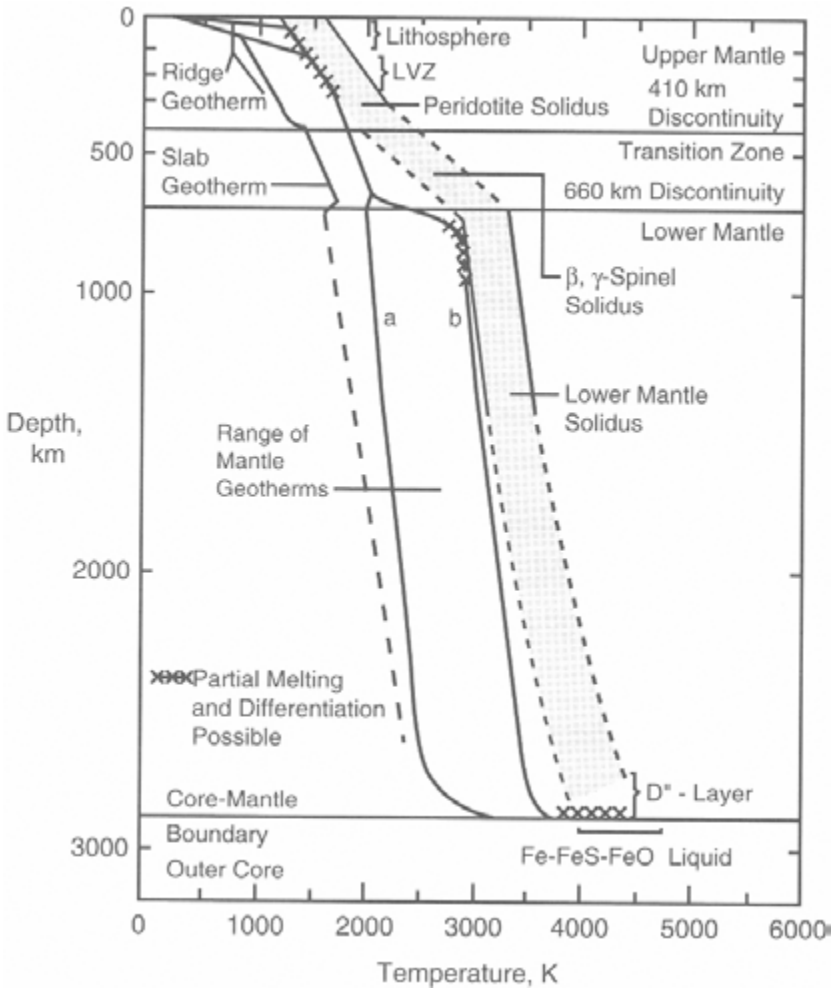

Figure 5. Summary of the plausible range of temperatures as a function of depth in the mantle [353]. LVZ = low-velocity zone.

of evidence: temperatures of magmas, the near-surface geotherm, geothermometers derived from mineral coexistences or solid solution compositions. At greater depths, temperatures can be constrained by the location of phase boundaries, such as the melting point of iron at 330 GPa and perovskite-forming transitions near 660 km depth. Thus, to examine the full range of phenomena (including melting) of relevance to the Earth's mantle requires experimental studies at conditions up to 135 GPa (1.35 Mbar) and temperatures up to ∼4500 K. The Earth's core covers an even more extreme range: 135–363 GPa and temperatures of perhaps up to 6000 K. These requirements place stringent demands on experimental apparatus to generate such conditions. The development of dedicated beamlines for high-pressure research at both second- and third-generation synchrotron sources has been a synergistic development which has not only led to advances in analytical capabilities but has also stimulated new developments in pressure- and temperature-generating apparatus. Both high-pressure tools and synchrotron experimental techniques are surveyed in the next section. Recent reviews of the applications of synchrotron research to materials research at high pressures can be found elsewhere [40, 41].

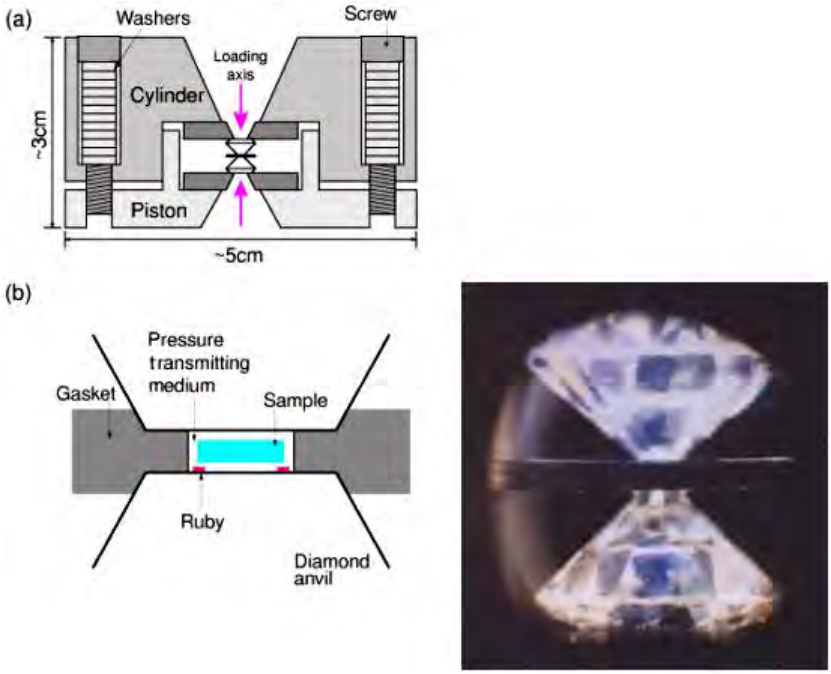

Figure 6. (Left) Schematic illustration of diamond anvil cell. (Right) Photomicrograph through a side opening in the cell showing diamond anvils and metal gasket between them.

3. Experimental techniques for planetary interior research

3.1. Apparatus for generating high pressure and temperature

3.1.1. Diamond anvil cell. In a diamond anvil cell, a sample is uniaxially compressed between two gem-quality diamonds (figure 6). Two advantages of the diamond cell have led to its widespread use in deep Earth studies: (1) very high pressures up to and beyond 100 GPa (1 Mbar) can be readily achieved; (2) the diamond windows are transparent across wide regions of the electromagnetic spectrum. The former means that, essentially, the entire pressure range of the Earth and terrestrial planets is accessible to direct study. The latter makes the diamond cell especially suited for *in situ* analyses, allowing application of a growing range of material probes.

The diamonds used in these experiments have flat culet surfaces that range from 0.05 to 1 mm in diameter depending on the pressure range of interest. Owing to the small surface area over which force is applied, only modest loading forces are required to achieve high pressures. The sample itself is contained within a small hole ($\sim$0.03–0.5 μm diameter) in a thin metal gasket placed between the anvils.

The main disadvantage of the diamond cell involves the small volume of compressed sample. For stable operation, the metal gasket between the anvils is initially thin ($\sim$30 μm) and plastic deformation with increasing load leads to further thinning such that at $\sim$100 GPa, the sample thickness may be only a few micrometres. The resulting sample chamber volumes decrease from dimensions of 10^{-2} mm^3 at $P \sim 10$ GPa to 10^{-5} mm^3 at $P \sim 100$ GPa. Thus, there is a requirement for highly sensitive analytical techniques and this has led to a natural marriage between high-brilliance synchrotron sources and the diamond anvil cell.

Measurement of equilibrium thermodynamic properties at high pressures and temperatures requires that the experiments be conducted under hydrostatic stress conditions. The uniaxial load in a diamond anvil cell is transformed to a hydrostatic pressure by surrounding the sample with a fluid pressure medium. However, above ∼16 GPa at room temperature, all known pressure media freeze, resulting in the development of some degree of non-hydrostatic stresses. In practice, samples are often surrounded by a soft solid pressure-transmitting medium, thereby generating a quasi-hydrostatic stress state. Rare gas solids (He, Ar, Ne) are often used for this purpose, but other soft materials (e.g. NaCl) are also employed. In addition, deviatoric stresses can be relieved by annealing the sample at high temperature using the laser-heating technique discussed later. Deviatoric stresses can often be readily monitored and characterized by measuring either the relative variations of lattice parameters or the ellipticity of diffraction rings together with lattice strain theory [42, 43].

Pressure measurement in the diamond anvil cell relies on the use of calibrated standards. One common method involves measurements of the R_1 fluorescence wavelength of small ruby crystals placed in the sample chamber excited using visible laser irradiation [44]. This ruby fluorescence scale [44–46] has been calibrated against room-temperature isotherms derived from shock Hugoniot data. The accuracy of the ruby scale has been verified to be within ±1% up to 55 GPa, from the analysis of simultaneous volume and elasticity data [47, 48], but its accuracy declines at higher pressures [49] and may also be affected by polymorphism of Al_2O_3 [50,51]. Some refinements to the ruby scale have been developed in recent years [52,53]. For synchrotron studies in both the DAC and multi-anvil apparatus (discussed later), the use of internal x-ray standards is common. The development of improved high P–T pressure standards is an important area of research [54].

Diamond anvil cell technology has undergone continual refinement since its inception. The needs of synchrotron experiments have driven the development of symmetric and panoramic cell designs [55], as well as improvements to x-ray transparent gaskets and backing plates [56, 122]. Earlier, nearly all diamond cell studies used an axial geometry in which the x-rays enter and exit the sample through the diamonds. However, a number of diffraction and scattering experiments require a wider range of angular access to the cell or suffer from excessive absorption by the diamonds (below ∼10 keV). The development of x-ray transparent beryllium [58, 59] and boron gaskets [60] have aided many experiments including diffraction experiments measuring lattice strain anisotropy in response to a non-hydrostatic stress field and inelastic scattering experiments using the panoramic geometry [55].

3.1.2. Laser heating. One of the most important developments resulting from the marriage of synchrotron beamlines and high-pressure techniques has been to foster *in situ* experiments at or approaching the P–T conditions of planetary interiors as opposed to the more indirect temperature-quench or ambient-pressure recovery experiments that dominated previously.

In the diamond cell, high temperatures can be achieved by electrical resistive heating or by laser heating. Resistive heating methods offer the advantage that they can produce highly uniform temperatures in the pressure cell, yet are often restricted to temperatures of ∼1300 K or less, thus, limiting the direct replication of geophysical conditions to those found in cold subducting slabs. Nevertheless, resistive heating methods have found important applications for pressure–volume–temperature (P–V–T) equation of state and phase transformation studies of planetary materials [61]. More recently, new designs for internal and external resistive heating have been developed that can reach either very high temperatures (∼3000 K) at modest pressures [62] or modest temperatures (1200 K) at megabar pressures with a high degree of thermal stability [63].

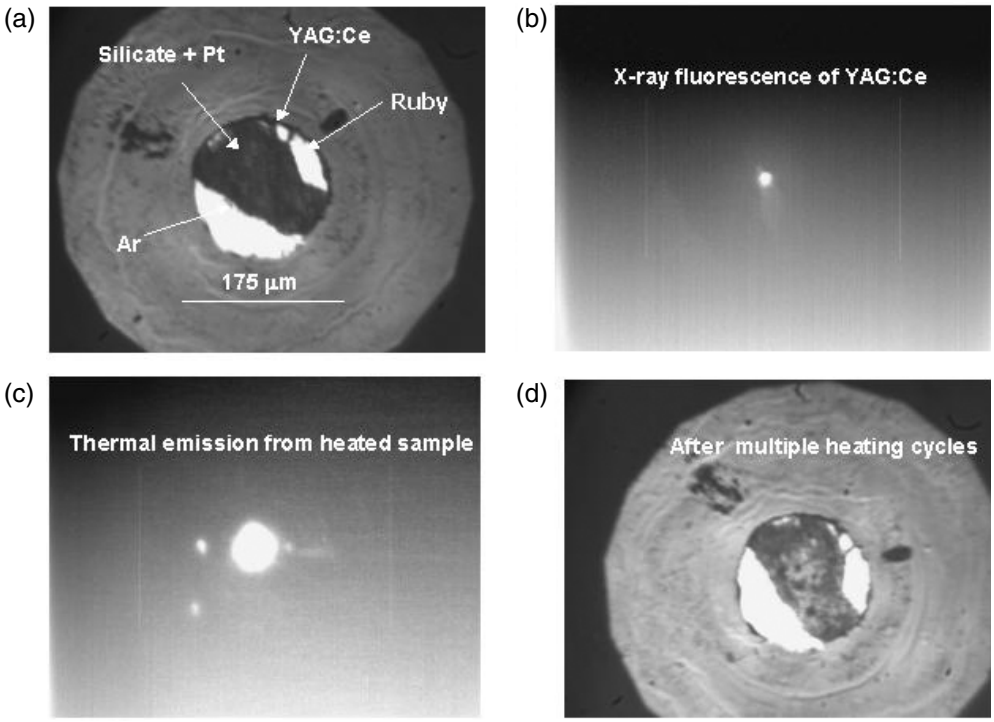

Figure 7. The laser-heated diamond anvil cell. (*a*) Sample viewed through the diamond anvils. The diamond culet is 500 μm in diameter. The sample consists of a mixture of a silicate (pyrope garnet) and platinum powder. The sample is insulated from the diamonds and surrounded by argon. Small ruby crystals and a cerium-doped YAG ($Y_3Al_5O_{12}$) crystal are also loaded into the sample chamber. The pressure is about 20 GPa. (*b*) The YAG : Ce crystals fluorescence in the visible (spectral emission range: 487–587 nm) in response to x-ray excitation. X-ray fluorescent crystals enable improved alignment of x-ray beam and heating laser [275]. (*c*) Visible radiation emitted by the heated sample at ∼2000 K. (*d*) Sample after several heating cycles. Pt diffusion away from hot spot produces an inhomogeneous distribution after repeated heating.

In the laser heating method, the sample is heated by an infrared (IR) laser beam and temperatures are measured by spectroradiometry [64, 65] (figure 7). This method has many advantages, among the most important of which is the ability to heat samples at high pressures to temperatures up to ∼5000 K. While different laser heating configurations have been installed at various synchrotrons, the double-sided heating design using a near-IR laser developed by Shen *et al* [66] is prominent at third-generation synchrotron sources such as the APS and SPring-8 [67, 68]. Systems using CO_2 laser sources have also been employed at synchrotrons [69, 70]. CO_2 laser heating systems have the advantage that the laser is directly absorbed by silicates and oxides, and no additional laser absorber is required. Concomitant with the development of dedicated laser heating systems at third-generation sources, there has been continual improvement in laser heating techniques, temperature measurement and sample assemblies [71]. In particular, efforts have been focused on the examination of thermal gradients [72–76], thermal pressure effects [77, 78] and chemical reactivity [79]. Characterization and improvements to the heating environment [57] and the optical system [70, 80] have also been the focus of recent work.

While laser heating can readily achieve planetary temperatures, it suffers from a serious disadvantage that strong radial and axial temperature gradients can develop. In modern laser heating systems, radial gradients are minimized in various ways including the use of TEM_{01} laser modes, combinations of low order (TEM_{00}, TEM_{01}) laser modes, multi-mode lasers or defocused beams. Micro-focusing of the x-ray beam to ∼5–10 μm diameter [81] can ensure that the diffracted intensity is restricted to the flat-topped portion of the sample hot spot.

A question with regard to laser heating has been the issue of systematic temperature uncertainties. These can arise from chromatic aberrations in the optical system [70], wavelength-dependent emissivity of the sample [64] and poorly characterized axial temperature gradients [76]. In the case of resistive heating, (and the large-volume apparatus discussed below), temperature measurements using thermocouples may also suffer systematic uncertainty owing to the poorly characterized effect of pressure on thermocouple voltage [82, 83]. Thus, an important advance is the recent development of an independent and absolute temperature calibration using the intensity ratio of phonon creation to phonon annihilation pairs as measured by nuclear resonant inelastic scattering on laser-heated samples [84,85]. At 1400 K and 24 GPa, the temperature from the phonon creation/annhilation sidebands could be determined to within 5–10% [85], and was in agreement with results from spectroradiometry [67, 85]. Further development of this method promises to provide improved temperature metrology under extreme conditions.

3.1.3. Large-volume apparatus. Large-volume multi-anvil presses cover a more limited P–T range than the diamond anvil cell. However, this disadvantage is compensated by a larger sample volume (∼1–10 mm^3) that allows for highly uniform (±10–20 K) and prolonged stable heating. More complex sample assemblages can be accommodated in this device as well. A variety of different anvil assemblies, including both single-stage and double-stage designs, are available. In a single-stage multi-anvil apparatus, pressures up to ∼15 GPa can be reached, whereas in double-stage systems conditions at the top of the lower mantle (∼30 GPa, 2000 K) can be achieved.

A major activity of the multi-anvil apparatus has been the quantitative determination of phase relations in multi-component systems that are relevant for the major lithologies expected in the mantle [19]. Before the development of synchrotron techniques, such studies were carried out on quenched samples. This approach has a limitation in that pressure is not well constrained at high temperatures. Other areas where the multi-anvil apparatus has played a prominent role include the determination of thermoelastic properties from ultrasonic interferometry [86], P–V–T equation of state [87], deformation studies [28] and properties of melts at high pressures [88].

A variety of press designs and characteristics can be found at various synchrotrons, and detailed descriptions of the multi-anvil systems at SPring-8 [89] and the Advanced Photon Source [90] have been reported. Another type of large-volume apparatus in use at synchrotron facilities is the Paris–Edinburg press [91]. The capabilities of large-volume apparatus systems continue to evolve rapidly. One recent technical development is the capacity of oscillating the press in the x-ray beam to improve diffraction crystal statistics in energy dispersive diffraction experiments [92]. The replacement of some or all of the tungsten carbide anvils with sintered diamonds or cubic boron nitride has been the focus of ongoing developmental efforts that have resulted in achievements of pressures in excess of 40 GPa at 2000 K [93] and in an improved x-ray access to the pressure chamber. Overviews of recent developments using synchrotron radiation and large-volume apparatus have been reported [83, 94].

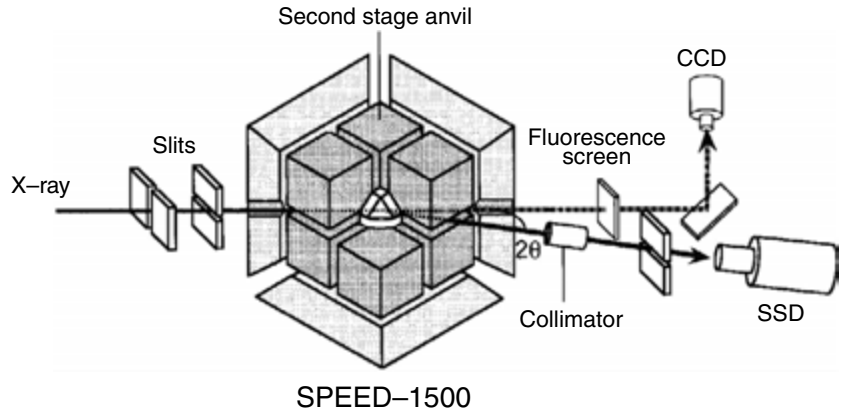

Figure 8. Experimental set-up for energy dispersive x-ray diffraction experiments in the multi-anvil apparatus. SPEED-1500 is an instrument in operation at SPring-8. From [83].

3.2. Synchrotron techniques for deep Earth studies

The development and growth of dedicated beamlines for high-pressure research at second- and third-generation synchrotron sources has enabled high-pressure studies to exploit a number of desirable characteristics of synchrotron radiation. High x-ray energies are valuable because of their ability to penetrate the pressure-confining medium. High intensities provide for rapid data accumulation on small weakly scattering samples. The small divergence of the beam enables achievement of small x-ray spots with slits or focusing optics that allow for higher intensities, isolate the pressure-confining medium and restrict the data collection to regions of minimal pressure and temperature gradients. The synchrotron developments have been coupled with developments in x-ray optics and detectors that allow detection of the subtle features often required to properly determine the unit cell and determine or refine the crystal structure. The tuneability of synchrotron sources and advances in high-resolution optics has allowed for development and application of resonant scattering and spectroscopic techniques.

3.2.1. Powder x-ray diffraction. Powder x-ray diffraction has been the workhorse technique for synchrotron-based high-pressure studies. Initially, the energy dispersive method was widely adopted [95]. In this technique, a white x-ray beam is directed through the diamond anvils or between gaps in the anvils of a multi-anvil apparatus and the diffraction is recorded as a function of x-ray energy at a fixed scattering angle using a solid-state detector (figure 8). The fixed scattering angle is well suited to high-pressure apparatus. In the diamond cell, supporting plates behind the diamonds have only limited opening angles, particularly for experiments aimed at achieving higher pressures. The energy dispersive technique allows for rapid, real-time data accumulation. Slits used for spatial filtering in the scattered beam path can reduce unwanted background scattering. However, the relatively poor energy resolution of solid-state detectors is a serious disadvantage, especially when examining lower symmetry phases or mixtures of multiple phases, as peak overlaps greatly hinder the data analysis. Also, as only a small portion of the diffracted cone is recorded, the measured intensities can be greatly affected by texture development under stress and grain growth during high-temperature experiments. Over the past two decades, energy dispersive diffraction has been a widely used technique for synchrotron-based studies of equations of state [43, 87, 96–101], high P–T phase

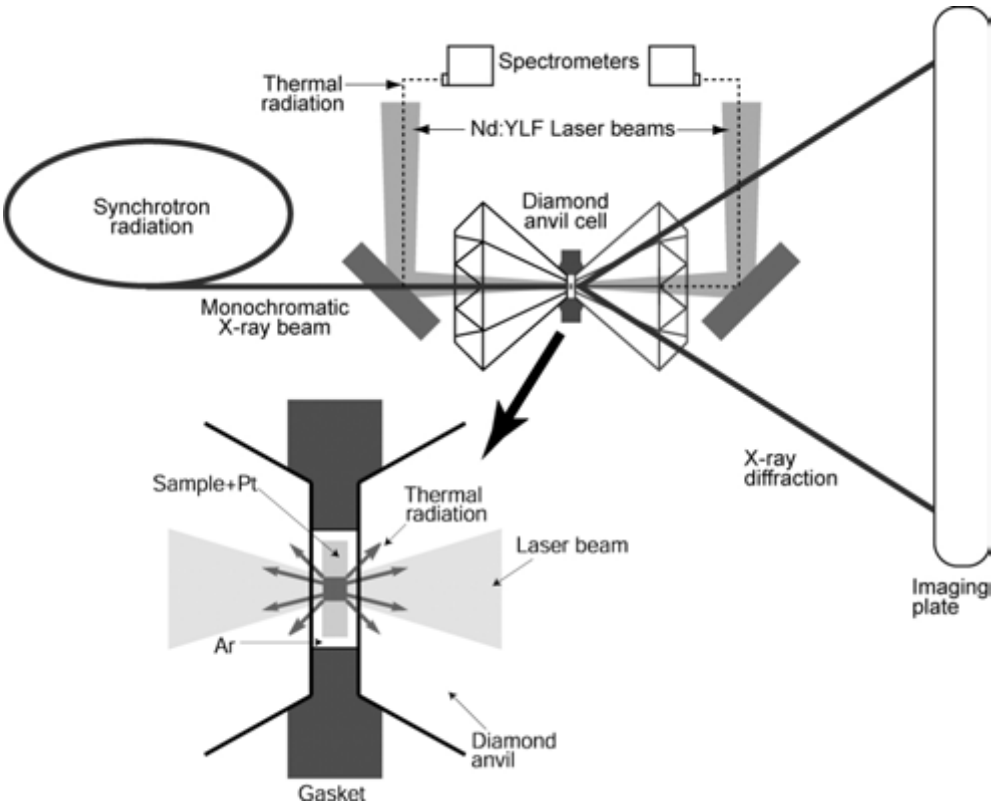

Figure 9. Experimental set-up for angle-dispersive x-ray diffraction experiments in the laser-heated diamond anvil cell. From [354].

transitions [102,103], texture development [58], strength and rheology determination [104,105] and melting studies [106].

The use of angle dispersive polycrystalline diffraction techniques at high pressures has increased in recent years. In this technique, a monochromatic x-ray beam is directed through the pressure apparatus and the rings of diffracted intensity are recorded using an imaging plate (IP) or CCD detector (figure 9). CCD detectors have the advantage that readout time is minimal which can be especially important for laser-heating experiments in the DAC. However, IPs have larger active areas, and superior resolution can be obtained. The main advantage of the angle dispersive method is markedly better angular resolution of diffraction peaks. Subtle phase transformations have been identified in several systems that could not be detected by the energy dispersive method (e.g. [107]). Also, with a CCD or IP detector, integration of the whole powder ring means that reasonable intensities can be obtained. The powder patterns can then be subject to whole profile structure refinements using the Rietveld method to obtain information on the evolution of structure parameters with pressure. An example of a Rietveld refinement result for the post-perovskite ($CaIrO_3$-type) phase in $MgGeO_3$ at 89 GPa is shown in figure 10. Area detectors also allow for the study of preferred orientation from which insights into deformation mechanisms can be obtained [108]. Time-resolved studies involving an IP translating continuously behind a slit, as the temperature is raised, can be used to obtain a single record across a high-temperature phase transition from which the kinetic parameters governing the transition can be recovered [109].

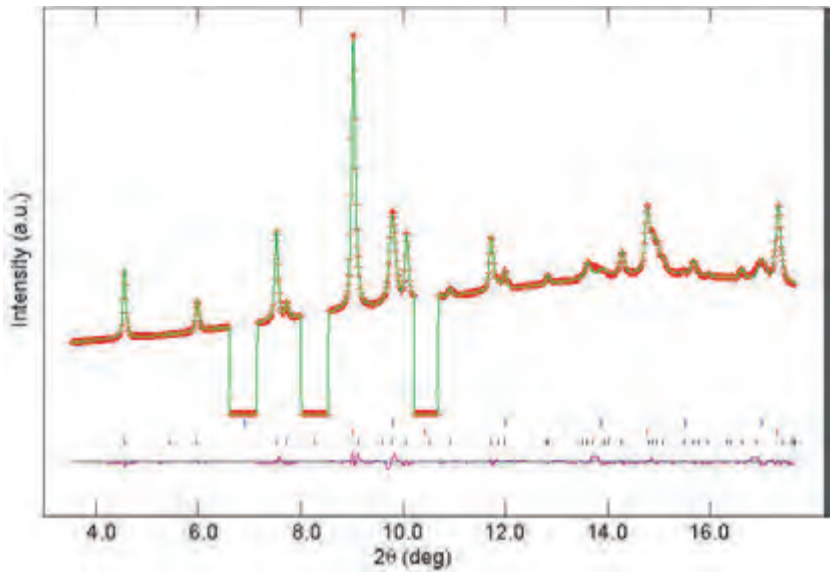

Figure 10. Representative Rietveld refinement results from monochromatic diffraction data for the $CaIrO_3$-type phase of $MgGeO_3$. The solid line shows calculated diffraction intensity and crosses are observed diffraction intensity. The pressure determined from the Pt (111) reflection is 89.0 GPa. The ticks at the bottom show diffraction peak positions for NaCl B2 phase (top), Pt (middle) and $CaIrO_3$-type $MgGeO_3$ (bottom). The curve below the ticks indicates the difference between the observed and the calculated diffraction intensity. Regions near 7°, 8° and 10.5° were excluded from the fit to avoid misfit due to deviatoric stress in Pt and NaCl and due to presence of ultratransformed starting material.

One disadvantage of the angle dispersive method is that the accessible d-spacing range may be limited by the constraints of the pressure vessel. The tuneability of synchrotron radiation can partially overcome this through the selection of relatively short-wavelength x-rays. Also, the loss of diffracted beam collimation means that diffraction from the pressure medium surrounding the sample and Compton scattering from the (diamond) anvils can lead to high backgrounds and low signal-to-noise ratio. A new technique that aims to combine the advantages of energy- and angle-dispersive diffraction by collecting angle-dispersive data, using a solid-state detector and white synchrotron radiation, has recently been developed for the multi-anvil press [110].

3.2.2. Single crystal x-ray diffraction. Single crystal experiments at high pressures are especially challenging owing to the limited access to reciprocal space afforded by the high-pressure apparatus. An energy dispersive single-crystal method for the diamond cell has been developed to overcome this limitation and give high accuracy in lattice constant determination under quasi-hydrostatic conditions at pressures that extend into the lower mantle range [111]. The spatial filtering of unwanted background owing to pressure cell components afforded by the energy dispersive technique is again effective for the case of very small crystals or very weak scatterers. Examples of applications of this method to mantle and core relevant materials include studies of FeO [112], $Mg(OH)_2$ [113] and SiO_2 [114]. Ferroelastic phase transformations in minerals that result in the softening of shear elastic moduli may have direct relevance for the interpretation of seismic shear velocities in the mantle [115]. In the case of SiO_2, determination of the precise cell constants from single-crystal diffractionprovides insights into the nature of the phase transition from stishovite to the $CaCl_2$-type phase [114]

while effects on strength and elasticity were obtained from other experiments using an energy dispersive diffraction in a radial geometry [116]. Another important geological application of this technique is to identify and characterize single-crystal inclusions in natural diamonds [117]. The technique has also been applied to the identification of high-pressure phases in meteorites. In the Shergotty meteorite, which is known to originate from Mars, the α-PbO_2 phase of SiO_2 was discovered and characterized [118]. This provides an interesting but not fully understood example of formation of metastable high-pressure phases in the SiO_2 system, a topic that has been addressed in detail in high P–T experiments, as discussed in a later section.

3.2.3. Synchrotron techniques for studying amorphous materials at high pressures. Melting is a major agent of chemical differentiation in planets. Silicate liquids exhibit complex behaviour under compression as the tetrahedral framework of the liquid adopts more compact configurations. The liquid structure, ultimately, determines the basic thermodynamic and transport properties of the melt, such as its viscosity and density. The geophysical consequences of such evolution can be profound. For example, melts generally have high compressibilities as compared with solids and this may lead to formation of regions on the Earth, where certain melts become neutrally or negatively buoyant (one possibility for this is the ultra-low velocity zone in the D$''$ region [5]). More generally, knowledge of melt and liquid properties bear on such processes ranging from those important to the Earth's formation and early evolution, such as magma ocean and core formation processes, to present phenomena such as surficial volcanic activity, and also the possible distribution of melts in the present mantle [119]. In the case of the Earth's core, melt properties allow constraints to be applied on chemistry of the core and convection and magnetic field generation in the outer core.

However, knowledge of the properties of melts and glasses is much more limited than for crystalline solids. Studies of glasses and quenched melts using a variety of techniques, such as NMR and IR spectroscopy, provide many insights which are ultimately indirect. Again, the development and improvement of synchrotron facilities has provided new opportunities for direct measurements at high pressures and temperatures.

X-ray diffraction measurements of local structure in liquids, using high-pressure devices, is especially challenging as the weak, broad scattering from the small compressed sample volume can be swamped by the background from the high-pressure apparatus. Synchrotron radiation has been crucial in making such measurements possible. Energy dispersive techniques, in which spectra are collected at a series of 2θ values, are effective because they allow for spatial filtering to reduce the background scattering [88]. Angle dispersive techniques provide more reliable intensities and have been developed using a multichannel collimator and a multi-anvil press [120]. Angle dispersive methods in the diamond anvil cell have been used to study the structural evolution of amorphous and liquid iron up to 67 GPa [121, 122].

Studies of liquid silicates are especially challenging because of their chemical complexity, low mean atomic number and high melting temperatures. Through a series of improvements to the energy dispersive method in a multi-anvil apparatus, x-ray diffraction studies [123] of $MgSiO_3$ and $CaSiO_3$ melts have now been reported at 6 GPa. Such studies enable the determination of the structural evolution of liquids and the degree of sharpness of structural changes and provide insights into compression mechanisms. While structural changes in liquids may be generally smooth, first-order liquid-to-liquid structural change have been observed in, for example, liquid phosphorus [124].

X-ray radiography methods [125] for density measurements of liquids, using x-ray absorption, have been used for liquid density determinations of potential planetary core materials at high pressures using a large-volume press. In this method, a reference sphere or cylinder is embedded in the liquid sample which is then illuminated with monochromatic x-rays. The

absorption contrast between sample and reference material can be used to determine the sample density to within ∼1% if several criteria are met. These criteria are that the materials of the pressure apparatus surrounding the sample remain homogeneous along the x-ray direction, the shape of the reference material (i.e. Al_2O_3) does not change with compression and the absorption coefficients are independent of pressure and temperature. The method has also been used to determine melt density in indium using the externally heated diamond cell [126].

Viscosities of liquid silicates have been extensively studied becuase of their importance for understanding magmatic processes in the crust and mantle [127]. Silicate melt viscosities are highly sensitive to changes in pressure reflecting changes in melt polymerization. An important advance in understanding viscosity in high-pressure silicate liquids was the development of the falling sphere method in which the measured terminal velocity of a rigid sphere falling through the liquid is related to viscosity through Stokes' law. Kushiro [128] carried out the first quench experiments in a piston-cylinder device and showed that, in contrast to normal liquids, the viscosity of silica-rich melts decreased with pressure up to 2.5 GPa. Using synchrotron radiation, an *in situ* Stokes' viscometry method has been developed in which radiography is used to record the motion of an x-ray opaque marker sphere [129]. This method has a number of advantages, especially the ability to determine more precise sinking velocities compared with fall-and-quench experiments. The pressure range of the technique applicable to silicate samples has now been expanded past 10 GPa and 2000 K as a result of advances in synchrotron capabilities and high-pressure techniques [130, 131]. While applications of such methods are still in the initial stages, examples of significant findings to date include confirmation of a viscosity minimum in liquid albite ($NaAlSi_3O_8$) near 5 GPa [131], and a direct test showing substantial disagreement between viscosities from the falling sphere method and those inferred from oxygen self-diffusion data for a silica-rich composition at high pressures [132].

3.2.4. X-ray scattering. While x-ray diffraction provides information on the static position of atoms, high-resolution inelastic x-ray scattering (IXS) techniques offer a means of probing lattice dynamics. IXS provides constraints on the dynamic structure factor and phonon dispersion over the entire Brillouin zone [133]. The experimental technique involves the use of a high-resolution monochromator-analyser system with energy resolution of ∼3 meV [134, 135]. Earlier, IXS techniques were of very restricted applicability at high pressures mainly because of constraints imposed by the pressure containment medium. The development of third-generation synchrotron x-ray facilities together with improvements in cell design has changed this situation. The high brilliance of the third-generation source coupled with improvements in efficient focusing optics now allows such techniques to be applied to samples as small as 10^{-4}–10^{-5} mm^3, resulting in the capability to perform such experiments in diamond cell samples up to the megabar range. Detailed discussions of the application of IXS to high-pressure research can be found elsewhere [134, 136].

For geophysical applications, synchrotron inelastic scattering experiments present significant new opportunities. Other techniques to measure phonon dispersion curves, such as inelastic neutron scattering, are generally feasible only at very low pressures or under other similarly restrictive conditions. In IXS, the sound velocities can be determined from the linear part of the acoustic phonon branches. The elastic wave velocities (and the corresponding elastic constant tensor) are crucial for deep Earth studies because of their direct connection to seismic profiles. More generally, the elastic constants give insight into mechanical and structural properties, material strength, mechanical stability, interatomic interactions and phase transition mechanisms. Methods such as Brillouin scattering and ultrasonic interferometry have been traditionally used for such measurements at static high pressure [137, 138]. IXS techniques provide a complementary approach that is free of some limitations, such as the

need for optically transparent samples in Brillouin spectroscopy. Polycrystalline IXS studies to date have focused on the determination of orientationally-averaged compressional sound velocities [134, 139]. The effects of preferred orientation on the average sound velocity must be taken into account [140]. Use of single crystals and measurements of both longitudinal and transverse phonons in various crystal directions can constrain some or all of the elastic tensor at high pressures [135, 141]. The application to crystals is limited only by the ability to preserve single crystals in a hydrostatic environment at very high-pressure conditions.

Nuclear resonant inelastic x-ray scattering (NRIXS) also provides information on elastic and vibrational properties including sound velocities and the (partial) phonon density of states (DOS) of samples containing Mossbauer isotopes such as ^{57}Fe [142, 143]. In this method the sample is compressed in a panoramic diamond anvil cell and the incident x-rays are focused to 5 μm by a Kirkpatrick–Baez mirror system. X-ray energies are scanned using a $\sim$1 meV tuneable monochromator, and multiple avalanche photodiodes are used as detectors [85]. High-pressure studies using this technique were reported on Fe up to 153 GPa at room temperature [144, 145]. From the phonon DOS, information on the vibrational heat capacity and entropy can be obtained, allowing for constraints to be placed on a variety of properties including the Gruneisen parameter and thermal expansivity, both of which are relevant for constraining the geothermal temperature gradient in planetary cores. NRIXS measurements have now been extended to simultaneous high pressure and high temperatures [67, 85, 146]. These are especially demanding experiments as the long (4–6 h) counting times and stringent thermal stability requirements of the experimental hutch ($\sim$5 mK h^{-1}) during NRIXS experiments require very stable heating systems and temperature control.

There are a number of complexities in the interpretation of NRIXS data. As with IXS, the determination of sound velocities requires some approximations in fitting of measurements. The NRIXS method constrains an average or Debye sound velocity. Extraction of compressional and shear velocities is complicated by elastic anisotropy which can be compounded by preferred orientation effects [147]. It is, therefore, somewhat difficult to put firm limits at present on the precision of the recovered velocities for both the NRIXS and IXS techniques. For samples containing other components in addition to iron, a partial DOSs associated with the iron sub-structure is measured, but this can be related to the Debye sound velocity of the whole sample [148]. A number of iron alloys that are candidate light elements for planetary cores have now been explored by NRIXS methods [149–151].

Synchrotron Mossbauer spectroscopy (SMS) is time-domain nuclear resonant scattering in the forward direction and is analogous to conventional Mossbauer spectroscopy in that it enables extraction of the hyperfine parameters (e.g. quadrupole splitting and isomer shifts) of Mossbauer-active nuclei. This method can be used to place constraints on properties such as valence states, local environment, site occupancies, magnetic properties of iron in minerals and high-pressure phases [152]. At elevated pressures, conventional energy-resolved Mossbauer spectroscopy is restricted to highly iron-rich samples, whereas the SMS technique is applicable to more diluted samples owing to the substantial increase in flux from synchrotron sources as compared with conventional gamma ray sources. Applications of SMS techniques at very high pressures include the study of hedenbergite at 68 GPa [153] and magnesium silicate perovskite at 120 GPa [152]. In Fe_2O_3, synchrotron Mossbauer spectra have been recorded on laser heated samples demonstrating a transitition from a low-temperature magnetic state to a high-temperature non-magnetic state at 24 GPa and 1000 K [154].

3.2.5. Spectroscopy

3.2.5.1. X-ray emission spectroscopy. In x-ray emission spectroscopy (XES), excitation of deep-core electrons produces fluorescent photons which are examined with sub-electronvolt

energy resolution [55]. An example of a geophysical application of XES is the study of the spin state of iron atoms through examination of the Fe K_β emission line. High spin–low spin transitions in Fe-bearing minerals can affect a number of physical properties including density and compressibility, geochemical behaviour (i.e. Fe partitioning among phases) and transport properties (thermal conductivity and electrical conductivity). Changes in the optical absorption spectrum could affect the dominant heat transport mechanism under deep Earth conditions by potentially enhancing radiative transfer [155]. In 1999, the first application of this method at high pressures was reported in which the high spin–low spin transition in FeS at 7 GPa was identified [156]. Numerous other materials have now been studied, even at conditions well above 100 GPa (e.g. [155, 157–162), and the geophysical implications of some of these studies are discussed later.

3.2.5.2. IR spectroscopy. Synchrotron radiation also provides a bright source in the IR region, and IR microspectroscopy systems at synchrotron beamlines can realize sensitivity several orders of magnitude of higher than conventional laboratory systems. Vibrational IR spectra recorded at high pressures complement diffraction data and yield information about bonding, crystal symmetry, phase transitions and vibrational properties. IR spectroscopy plays an important role in elucidating the behaviour of hydrogen in Earth minerals. There has been considerable interest in the various hydrated mineral systems and their geophysically relevant properties as discussed earlier. Examples of application of IR spectroscopy to these phases include the study of brucite [163] and chondrodite [164] at elevated pressures. More detailed reviews of the applications of high-pressure IR micro-spectroscopy are reported elsewhere [165, 166].

4. Selected applications of synchrotron research to the mantle

4.1. Equation of state

Interpretation of seismic structure of the Earth began more than 50 years ago when Birch [167] recognized that phase transitions or chemical changes were necessary to explain the seismic structure of the upper mantle. The crystal structure and the equation of state of each candidate mineral at high pressures and temperatures are the most basic information needed to model the mineralogy of the mantle. High P–T structural studies using synchrotron x-ray diffraction have long played a key role in identifying stability ranges of minerals phases [61]. Among experimental methods that constrain elastic properties, static P–V compression experiments [168] have been a major contributor as they can be applied across the widest range of P–T conditions and have no special sample requirements, making them feasible even on non-quenchable high P phases. Nevertheless, equation of state determination needs to be performed with care. At room temperature, the effects of non-hydrostatic stress can bias equation of state parameters. Also, the well-known trade-off between fit values of the bulk modulus and its pressure derivative needs to be considered. P–V–T equation of state measurements provide constraints on thermal parameters required to model mineral assemblages at high-temperature interior conditions [87]. At high temperatures, the parameters that govern the thermal equation of state can be recovered with varying degrees of precision from different experimental tools which can sample different P–T ranges with variable levels of experimental precision [169, 170].

4.2. Phase changes and seismic discontinuities in the upper mantle

The development of *in situ* synchrotron x-ray techniques at mantle pressures and temperatures has provided an opportunity for a more direct investigation of phase changes in mantle minerals and their connection to seismic discontinuities. *In situ* phase boundaries by synchrotron x-ray diffraction are complementing and increasingly supplanting understanding of basic phase relations of the deep Earth which earlier had been based almost entirely on quench studies (e.g. [19]). The pioneering synchrotron studies of silicate phase transformations are yielding a considerably revised picture of phase boundaries in the $(Mg,Fe)_2SiO_4$ binary system and other mantle relevant systems. Further, synchrotron studies promise to greatly improve constraints on transition pressures and temperatures, widths of phase loops, behaviour of chemically complex system and, finally, understanding of transformation mechanisms and kinetics.

4.2.1. 660 km discontinuity. The 660 km discontinuity has long been associated with the transformation in $(Mg,Fe)_2SiO_4$ from the spinel phase (ringwoodite) to a post-spinel assemblage of $(Mg,Fe)SiO_3$ perovskite and (Mg,Fe)O ferropericlase, as found in quench experiments [171]. A surprising result was that the first *in situ* determination of the post-spinel phase boundary in Mg_2SiO_4, using synchrotron diffraction in a multi-anvil apparatus, yielded a pressure for the transformation that corresponded to a depth of only ∼600 km at 1600°C [172]. Other studies, using similar techniques, also reported unexpectedly low transition pressures in Mg_2SiO_4 [22] and $Mg_3Al_2Si_3O_{12}$ [173]. The effect of ∼10 mol% Fe is expected to only lower the transition pressures further.

These findings suggest that either the 660 km discontinuity is not associated with the post-spinel transition or that there are unresolved experimental issues associated with the *in situ* synchrotron experiments. Most follow-up studies have focused on exploring high P–T synchrotron techniques, and alternative models for the discontinuity have not been seriously considered (see [173] for an exception). The most likely explanations for the discrepancy involve the uncertainty in pressure calibration at high temperatures or error in temperature measurements owing to the uncertain effect of pressure on thermocouple emf [82, 174, 175].

The first synchrotron diffraction study [176] of the post-spinel phase boundary, using the diamond anvil cell, instead found good agreement with the expected pressure of the discontinuity based on seismology, consistent with another diamond cell study using Raman spectroscopy as a diagnostic [177]. One of the main differences between the two diffraction studies involved the P–V–T equation of state for the *in situ* pressure standard. The initial result of Irifune *et al* [172] was based on a particular equation of state (owing to Anderson *et al* [178]) for the gold internal standard. However, a number of thermal equations of state for gold have been proposed and there are discrepancies among them [178–180]. The results of Shim *et al* [176] were based instead on the equation of state of MgO [181] and Pt [182].

The post-spinel phase boundary in Mg_2SiO_4 was also re-investigated recently, using both *in situ* diffraction and quench techniques in the multi-anvil press by Fei *et al* [183]. This study employed multiple internal pressure standards. When the Au scale of Anderson *et al* [178] is used as an internal calibrant, the phase transition occurs at pressures below those corresponding to the 660 km discontinuity, in agreement with Irifune *et al* [172]. However, the use of MgO as an internal standard [181], results in close agreement between the pressure of the transition and that of the 660 km boundary in Earth's mantle, which is generally consistent with the findings from the diamond anvil cell experiments [176]. Recently, new Au pressure scales have been proposed [54, 184] and these appear to be in better agreement with results based on the MgO scale.

Table 1. Clapeyron slopes of Olivine phase transformations.

Composition	Phase transition	*In situ* measurement (MPa K^{-1})	Quench (MPa K^{-1})	Reference
Mg_2SiO_4	$\alpha \longrightarrow \beta$	4.0	—	[191]
$(Mg,Fe)_2SiO_4$	$\alpha \longrightarrow \beta$	3.6	—	[22]
$(Mg,Fe)_2SiO_4$	$\alpha \longrightarrow \beta$	—	2.5	[196]
Mg_2SiO_4	$\beta \longrightarrow \gamma$	6.9	—	[197]
Mg_2SiO_4	$\beta \longrightarrow \gamma$	—	5.0	[196]
Mg_2SiO_4	$\gamma \longrightarrow$ pv + fp	−1.3	—	[183]
Mg_2SiO_4	$\gamma \longrightarrow$ pv + fp	−0.4 to −2.0	—	[175]
Mg_2SiO_4	$\gamma \longrightarrow$ pv + fp	—	−3.0	[171]

pv = (Mg, Fe)SiO_3 perovskite, fp = (Mg, Fe)O.

In situ x-ray diffraction studies also place constraints on the Clapeyron slope of the post-spinel transition in Mg_2SiO_4. The slope reported by Fei *et al* [183] was $-1.3\,MPa\,K^{-1}$, while Katsura *et al* [175] reported values ranging from -0.4 to $-2.0\,MPa\,K^{-1}$. Both of these results are lower than the previous determinations ($\sim -3.0\,MPa\,K^{-1}$) based on quenching experiments [171] and calorimetric studies [185] (table 1). The difference between quench and *in situ* experiments may be related to temperature effects on the calibration curve used to determine pressure in the quench experiments, or because of the sluggish reactions kinetics at low temperatures [175]. A less negative Clapeyron slope for the post-spinel transition will make this transition less effective in impeding material transport across the phase boundary [24], and thus favours large-scale mixing of material between the upper and lower mantle. The Clapeyron slope is also used to estimate lateral thermal variations in the mantle associated with lateral variations in the depth to the discontinuity. Using the new synchrotron Clapeyron slope measurements, the observed ±20 km variations of the depth to the discontinuity [186, 187] correspond to lateral temperature variations of ±400 K or more [175], which is considerably greater than the earlier estimates (∼250 K) based on the Clapeyron slope from quenching experiments.

Synchrotron diffraction studies using the multi-anvil apparatus have also been used to investigate phase boundaries near 660 km depth in $MgSiO_3$ [188, 189] and $Mg_3Al_2Si_3O_{12}$ [173]. In addition, the phase relations in a pyrolite composition were examined at conditions near the 660 km discontinuity, using a combination of synchrotron x-ray diffraction and quench studies [190]. The latter study found that the post-spinel transition in a pyrolite composition at 1600°C is still about 1.5 GPa (or ∼40 km) below the expected pressure of the 660 km discontinuity even when a more recent gold pressure scale [184] is adopted. Further studies to develop more accurate pressure scales and to investigate other systematic error sources in high P–T experiments are clearly needed to better understand the depths, slopes and widths of mantle-relevant phase transformations.

4.2.2. 410 km discontinuity. The first synchrotron-based *in situ* study of the olivine(α)–wadsleyite(β) transformation was carried out on end-member Mg_2SiO_4 [191]. More recently, Katsura *et al* [22] carried out a comprehensive analysis of the olivine-to-wadsleyite phase transformation in the binary $(Mg,Fe)_2SiO_4$ system. In this case, pressure was determined by *in situ* x-ray diffraction, using recent MgO pressure scales [181, 192, 193], while the phase relations were determined by the analysis of quench products from a large-volume press. As this study considered compositions spanning likely Fe abundance in the upper mantle, more direct geophysical constraints on the phase boundary could be obtained. By comparison of

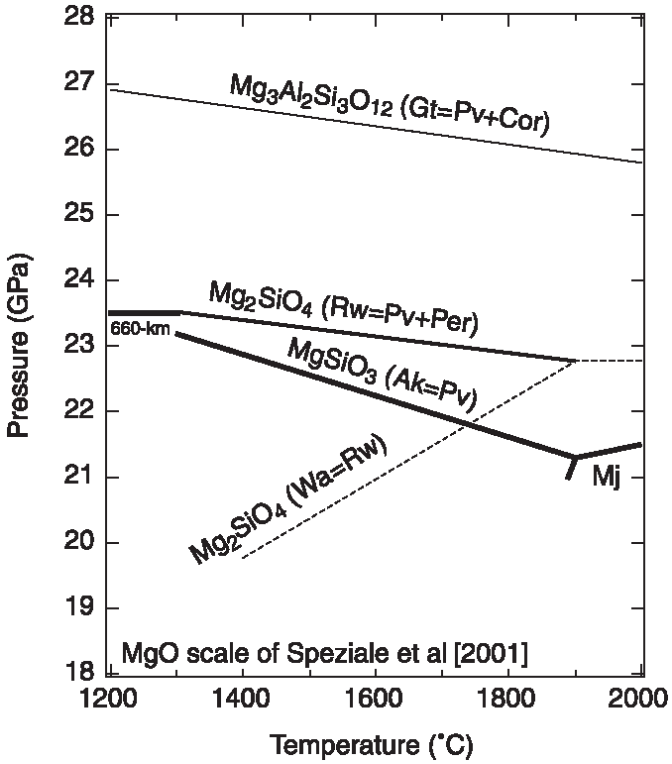

Figure 11. Phase boundaries for selected transitions involving end-member mantle minerals from *in situ* synchrotron diffraction studies. Abbreviations are: Gt—garnet, Pv—perovskite, Cor—corundum, Rw—ringwoodite, Per—periclase (MgO), Ak—akimotoite, Wa—wadsleyite, Mj—majorite. From [183].

the measured Clapeyron slope of the transitions with the pressure expected at 410 km depth, the temperature at this depth was estimated to be 1760±45 K for a pyrolitic mantle, and this, in turn, corresponds to a mantle potential temperature of 1550–1650 K. This compares favourably with the potential temperature of ∼1600 K estimated independently from mid-ocean ridge basalt (MORB) chemistry [194].

The slope of the α–β transition was found to be 3.6–4.0 MPa K^{-1} in synchrotron-based experiments [22, 191], whereas earlier results from quench experiments and calorimetry had yielded lower slopes [195, 196]. Interestingly, the Clapeyron slope for the β–γ transition in Mg_2SiO_4 from *in situ* diffraction (6.9 MPa K^{-1}) [197] is also greater than that observed in quench studies. Together with results for the 660 km discontinuity discussed earlier, the *in situ* synchrotron-based measurements consistently yield more positive and less negative slopes for these phase boundaries as compared with results from quench experiments and calorimetry (figure 11 and table 1). A possible explanation is that the amount of pressure decrease with heating was systematically overestimated in quench experiments [22].

Gu *et al* [186] mapped the global variations of the depth to the 410 km discontinuity at long seismic periods and found variations of the order of 5 km. Based on the recent synchrotron Clapeyron slope determination, this would correspond to thermal variations of ∼50 K [22]. Flanagan and Shearer [187] found larger variations of ∼22–27 km with little correlation with surface tectonics. This would correspond to the thermal variations of ∼250 K at this depth.

However, there is also little correlation between the tomographic maps of seismic velocity variations and the discontinuity topography. The topography of the discontinuity could also reflect variations in Mg# of olivine. Higher Mg# results in faster seismic velocities. Thus, topgraphic variations at 410 km depth could reflect a combination of thermal and compositional effects.

The new synchrotron diffraction data also allow for a comparison of the thickness of the olivine–wadsleyite transition with that found for the 410 km discontinuity by short-period seismic data. In order to make this comparison, the change in Fe across the transition owing to different partitioning behaviour of olivine and wadsleyite must be included [198, 199]. While the effect of nonlinearity on the yield of wadsleyite, as the transition proceeds, was found to be small, latent heat increases the width of the transition to some extent [22]. The end result is that the thickness of the olivine–wadsleyite transition is expected to be between 7 and 13 km, which is considerably greater than that found by short-period seismic observations (thickness <5 km [200, 201]). To provide an explanation for this discrepancy, Katsura *et al* [22] proposed that the mantle near 410 km depth is depleted in olivine (∼40%) as compared with pyrolite (∼60% olivine) and has an Mg# of ∼0.89. This would reduce the width of the discontinuity to ∼5 km, while also providing a better match for the magnitude of the seismic velocitiy discontinuity [21]. Possible changes in chemical composition across the 410 km discontinuity, especially enhanced incorporation of hydrogen in the wadsleyite phase, may also affect the width of the discontinuity and the velocity contrast [199].

4.3. Slab penetration into the lower mantle

Seismic tomographic images show that some subducting slabs penetrate unimpeded across the 660 km discontinuity and into the lower mantle whereas others appear to stagnate in the transition zone [8]. The different behaviour of slabs could be related to their age and thermal structure: older slabs are colder and thicker than younger slabs and, therefore, are more likely to penetrate into the lower mantle. The subducting oceanic plates consist of a basaltic crust and underlying lithospheric mantle. The behaviour of the two layers may differ because of their different composition. The subducted oceanic crust remains appreciably denser than the surrounding mantle up to at least 600 km depth. However, it has been suggested that eclogite, the high-pressure form of basalt, becomes neutrally buoyant near the boundary between the upper and lower mantle as a result of the survival of garnet in basalt compositions to higher pressures before transformation to perovskite [202]. This could lead to separation of the basaltic crust and its accumulation in a 'garnetite' layer near the top of the lower mantle [203, 204] (figure 4). These ideas have recently been tested on basaltic compositions using quench experiments [205] and *in situ* synchrotron x-ray diffraction [206] with multi-anvil apparatus. Both studies suggest that the transformation of basalt to a perovskite-dominated lithology occurs at relatively shallow depths (<720 km), and there would be little driving force for gravitation separation of basalt from peridotite. However, differences in reaction rates between the garnet–perovskite and spinel–perovskite transformations could be important. Recent synchrotron x-ray diffraction experiments have examined the phase transition kinetics by directly measuring the rates of transformation. Kubo *et al* [207] found that the kinetics of the garnet–perovskite transformation are much slower than those of the spinel–perovskite transformation. It was concluded that appreciable amounts of metastable garnet might survive on geological timescales ($\sim 10^7$ yr) in the descending cold oceanic crust under lower mantle conditions. Thus, if metastability is important, the buoyancy of oceanic crust at the top of the lower mantle would be enhanced, possibly allowing for the formation of a garnet-rich layer.

4.4. Mantle rheology

Rheological properties of mantle mineral are necessary for understanding the mechanism of solid-state convection in the Earth, and for exploring such phenomena as the origin of deep focus earthquakes. However, quantitative studies of rheological properties of materials at high pressure have generally been limited to 4 GPa or less, corresponding to depths of less than 120 km. Thus, only the conditions at the top of the upper mantle have been the subject of direct examination. Consequently, there is little direct understanding of how deformation behaviour may change with pressure and temperature. In the last few years, however, new synchrotron-based techniques have allowed for quantitative studies of high-pressure strength and mantle rheology at *in situ* conditions for the first time.

The diamond anvil cell can be used as a deformation apparatus. In early studies, the yield strength of materials was inferred from measurements of pressure gradients across the sample (e.g. [208, 209]). The development of methods for measuring and interpreting lattice strain anisotropy, using x-ray diffraction in a radial geometry with x-ray transparent gaskets [42,210], has led to significant advances in the characterization of low-temperature strength, elastic anisotropy and texture development in materials of geological interest. P–V measurements performed at a 'magic angle', with respect to the loading axis, allow for determination of the quasi-hydrostatic equation of state from data under non-hydrostatic conditions [104,211]. Yield strengths have been determined to ∼70 GPa for a number of silicates, oxides and metals (figure 12) [104, 105, 211]. As a result of work hardening at these large strains, the ratio of differential stress or yield strength, Y, to shear modulus, G, increases with pressure, contrary to predictions of constitutive strength models that assume linear scaling [212]. For silicates and oxides, systematic trends in strength are apparent. At lower pressures, the yield strength of four-coordinated upper mantle minerals, such as olivine and ringwoodite, is in the range of 4–6% of the shear modulus. The strength of six-coordinated silicates ($CaSiO_3$, stishovite, $MgSiO_3$) is lower and amounts to ∼3–4% of the shear modulus at lower mantle pressures. Measurements up to 300 GPa show that differential stresses up to 10% of the pressure can be developed in strong metals under these ultra-high P conditions [59]. Elastic constants can also be recovered from radial x-ray diffraction experiments [105,116] (figure 13), although in some cases these may be affected by plastic anisotropy [213].

In the multi-anvil press, although the loading is hydrostatic, a deviatoric stress field in the sample is created by the anisotropy and strength of the sample assembly. One class of deformation experiments that has been developed and refined in recent years involves compressing a sample to generate local stress heterogeneity that manifests itself as a broadening of diffraction peaks [27]. By heating the sample and monitoring the resultant stress relaxation with time-resolved x-ray diffraction, empirical flow laws can be developed [214]. Weidner *et al* [26] have used this method to examine the strength of different mantle minerals under subduction zone conditions and have shown that the temperature dependence of strength is quite variable among the major subduction zone phases. In particular, while perovskite is weaker than ringwoodite at room temperatures (in agreement with diamond cell data), it is stronger at high temperatures [215], and this may have a bearing on earthquake processes in subduction zones.

A new device for rheology studies is a modified Drickamer-type apparatus, in which one anvil has the capability to rotate [216]. The sample is then deformed in simple shear between the two pistons yielding the possibility of achieving very large strains. Another new type of multi-anvil deformation device is called the D-DIA [217]. In the D-DIA, two of the six anvils are able to move independently, allowing for the application of a differential stress, while maintaining a fixed confining pressure. Differential (elastic) lattice strain is measured by distortion of Debye

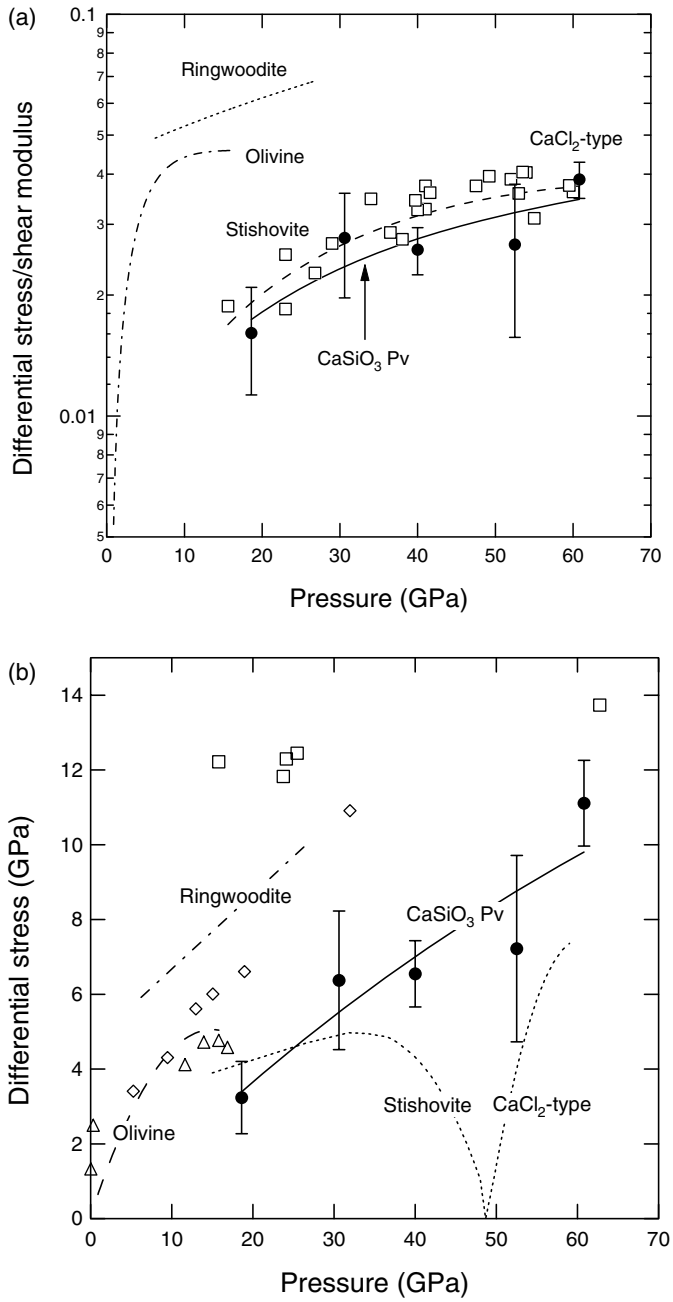

Figure 12. Strength of mantle silicates at lower mantle pressures and 300 K [105]. (*a*) The ratio of differential stress (yield strength) to shear modulus for $CaSiO_3$ perovskite (●) [105], ringwoodite [220], olivine [355] and SiO_2 (□) [116] from radial diffraction experiments and lattice strain theory. The stishovite-$CaCl_2$-type phase boundary is near 50 GPa. (*b*) 300 K yield strength of mantle silicates. Data for perovskite compositions close to $(Mg_{0.9}Fe_{0.1})SiO_3$ shown as open squares [356], open triangles [215] and open diamonds [357].

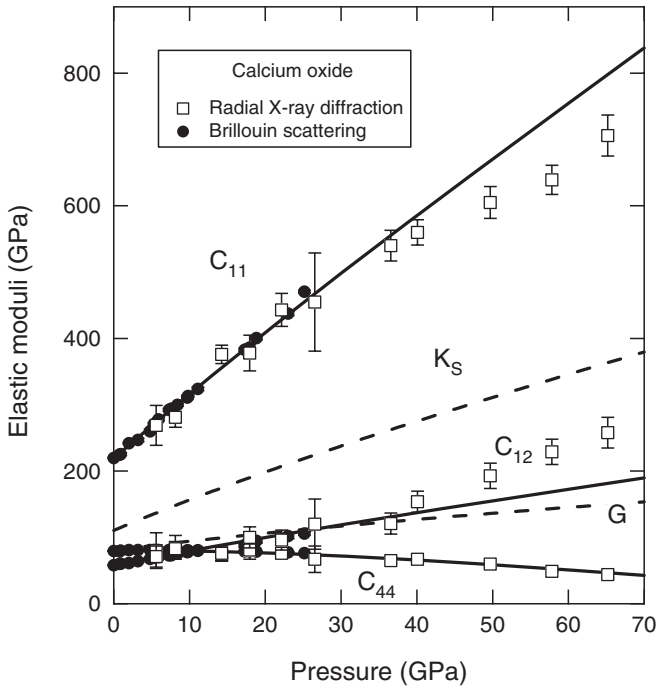

Figure 13. Elastic constants of CaO at high pressures from Brillouin scattering and radial x-ray diffraction. X-ray diffraction and Brillouin scattering results are in excellent agreement over the common pressure range (at 24 GPa) and the x-ray results even capture the softening of C_{44} with pressure. The radial diffraction results agree with extrapolation of Brillouin results at 40 GPa but diverge at higher pressures for C_{11} and C_{12}.

rings, and total axial strain (which may include a significant plastic component) is monitored by radiography. This device promises to provide a more complete characterization of rheological behaviour as lattice strain can be examined as a function of pressure, temperature, strain rate and total plastic strain. As examples, ringwoodite and MgO have been examined at high pressures with this device documenting pressure, temperature and strain dependence of the strength [218, 219]. The D-DIA results show that earlier studies [35, 220] of low-temperature strength of ringwoodite can be rationalized by accounting for differences in work hardening that result from different strain levels in the D-DIA, diamond cell deformation and multi-anvil stress relaxation experiments.

4.5. Lower mantle minerals

Experimental studies have shown that the mineral assemblage adopted by a peridotite lithology under lower mantle conditions consists of three main minerals: (Mg,Fe)SiO_3–Al_2O_3 perovskite (Mg-pv), $CaSiO_3$ perovskite (Ca-pv) and (Mg,Fe)O ferropericlase (fp) [221–224]. In the lower mantle, basaltic compositions consist of two perovskites, a stishovite and an additional aluminous phase [205, 225]. In this section, synchrotron-based experimental studies of major lower mantle minerals of basalt and peridotite compositions are reviewed.

4.5.1. Magnesium silicate perovskite. As the expected dominant phase of the lower mantle, the properties of magnesium silicate perovskite, (Mg,Fe)SiO_3, have attracted much attention.

Initial synchrotron diffraction experiments using energy dispersive techniques in both the diamond anvil cell and large-volume press focused on the thermal equation of state [226–228]. Subsequently, higher resolution diffraction studies extended equation of state and structural determinations to 94 GPa [229, 230]. The stability of perovskite was demonstrated at 106 GPa (2300 km depth conditions) by *in situ* measurements [231, 232], which also reported evidence for a possible modification of the perovskite structure [231]. Earlier reports [102, 233, 234] of breakdown to oxides or transformation to a cubic perovskite at ∼60–80 GPa were not confirmed by later studies.

Mineralogical models for the Earth's mantle typically contain ∼4–6 mol% Al_2O_3. The effects of aluminium incorporation on the structure and physical properties of perovskite have been a subject of much interest. P–V EOS measurements suggested that the presence of 5 mol% Al_2O_3 lowers the bulk modulus of $MgSiO_3$ perovskite by ∼10% [235], a surprising result that is contradictory to expectations from elasticity systematics. Many additional P–V EOS studies of Al-bearing perovskites have subsequently been reported, but the results are highly variable with both increase and decrease as well as no changes in compressibility reported [236–241]. The results seem to depend in a complicated manner on synthesis conditions as well as the substitution mechanism and its evolution. The difficulty of accurately constraining the bulk modulus from volume compression data owing to parameter tradeoff, limited compression range, deviatoric stress, etc may also play a role here. Interestingly, recent high-pressure polycrystalline Brillouin scattering measurements, which place more direct constraints on the bulk modulus, found no difference in compressibility between Al-containing and Al-free perovskite samples, but rather found a 6% reduction in the shear modulus of the Al-containing sample [242]. Variations in aluminium content are thus a possible explanation for lateral heterogeneities in the lower mantle that exhibit large relative variation in shear velocity compared with compressional velocities.

X-ray emission spectra measurements indicate that magnesium silicate perovskite undergoes an electronic transformation from a high-spin to a low-spin state, at lower mantle pressures [155, 160]. Data for $Mg_{0.9}Fe_{0.1}SiO_3$ showed the presence of electronic transitions corresponding to partial and full spin pairing at 70 GPa and 120 GPa, respectively [155]. The former corresponds to a depth range (∼1700 km), where a similar transformation is observed in (Mg,Fe)O (see later) and where seismic studies begin to suggest the existence of possible chemical heterogeneities [29]. The second transition is close to the boundary of post-perovskite phase transition (also discussed later). Another study using the same method on Al- and Fe-containing samples found evidence of a continuous transition from high spin to low spin over a broad pressure range, with a mixed spin state being observed at ∼100 GPa [160]. Such spin pairing transitions are potentially significant for interpreting geophysical data in the deep lower mantle as resulting changes in physical properties (e.g. thermal expansivity, thermal conductivity) could act to decrease mixing rates and thereby help to maintain chemical heterogeneities, but this depends in detail on the P–T evolution of the transition.

The geophysical and geochemical properties of the Earth's deep interior depend on the partitioning of iron between the major Fe-bearing lower mantle phases: $(Mg,Fe)SiO_3$ perovskite and (Mg,Fe)O ferropericlase. Partition coefficients can be determined from synchrotron x-ray diffraction studies of volumes of coexisting phases [243, 244] or by transmission electron microscopy (TEM) analysis of samples recovered at ambient conditions [245, 246]. At pressures at the top of the lower mantle, iron is preferentially partitioned into ferropericlase, but there are conflicting reports on the trend with pressure as diffraction-based measurements conclude that Fe^{2+} is increasingly allocated into perovskite with depth [243, 244] whereas TEM-based studies find no significant change in the partitioning

behaviour [245,246]. A number of factors including pressure, temperature, aluminium content, ferrous/ferric ratios and spin states may affect the partitioning behaviour. Constraining partition coefficients in complex assemblages under such extreme conditions remains a foremost challenge in high-pressure mineral physics.

4.5.2. Calcium silicate perovskite. A $CaSiO_3$-rich perovskite phase is expected to exist under lower mantle conditions and it was long thought that this phase possesses cubic symmetry [247–249]. A number of energy dispersive diffraction experiments have been carried out on the material since 1989. These studies are mainly focused on the room temperature and thermal equations of state and are a good example of the continual improvements in data quality that have been realized through advances in experimental techniques and synchrotron capabilities over the last fifteen years [101, 105, 247–251]. Recently, an angle dispersive x-ray diffraction study [107] showed for the first time that the symmetry of $CaSiO_3$ perovskite at room temperature is not cubic, but tetragonal or orthorhombic, in agreement with theoretical predictions [252–254]. This was confirmed in subsequent diffraction studies but these also showed that the cubic form is stable under high temperature–high-pressure conditions [224, 246, 255, 256]. The transition temperature was found to increase with the aluminium content of the samples, and it is plausible that a transition from cubic to a lower symmetry form may occur under some lower mantle conditions. Such a transition is likely to be accompanied by significant anomalies in elastic properties [254] and may, therefore, have relevance for the interpretation of seismic profiles.

4.5.3. (Mg,Fe)O. The behaviour of the (Mg,Fe)O system illustrates how even simple mineral systems can show complex behaviour under extreme conditions. The endmember, MgO, remains stable as the rocksalt (B1) structure at at least 227 GPa [43] and its equation of state has been sufficiently well characterized using a variety of experimental [181, 257] and theoretical methods [192, 193] to make it perhaps the best documented *in situ* pressure standard [54]. However, at room temperature, $Fe_{1-x}O$ undergoes a rhombohedral distortion above ∼17 GPa depending on the level of deviatoric stress [258] and transforms to the NiAs (B8) structure at ∼75 GPa and high temperatures [259,260]. While the (Mg,Fe)O series exhibits complete solid solution at ambient pressure, the different behaviours of the end-members suggest complexities could appear in the phase diagram at high pressures and temperatures. The rhombohedral distortion has also been observed in Fe-rich solid solutions ($Mg\# = Mg/(Mg + Fe) < 0.2$) [261, 262], but the transformation to the B8 structure has not been observed at megabar pressures in any composition except for the Fe end-member [261]. Evidence from x-ray diffraction experiments suggests that intermediate compositions (Mg#50–80), at least partially, dissociate at conditions near 83–86 GPa and 1000 K to an Mg-enriched composition and an almost pure wustite (FeO) composition [263, 264]. A dissociation transition in the Earth's mantle would produce phases of considerably different density and may well affect the dynamics and chemistry of the lower mantle [2, 29]. However, other diffraction experiments on more Fe-rich compositions (Mg#39 and Mg#25) at 86–102 GPa and 2500 K did not find any evidence of dissociation or transformation to the B8 structure [265]. Experiments on peridotite compositions up to 124 GPa have also not reported evidence of dissociation [246].

A high-spin to low-spin transition in Fe has been reported using XES in an Mg#83 composition at 50–60 GPa, but this was not accompanied by any abrupt change in the structure or volume [159]. Such a transition could change Fe partitioning and partial melting behaviour in the lower mantle. In contrast, XES measurements on $Fe_{0.92}O$ showed no transition to a low-spin state for pressures as high as 143 GPa [157]. Further studies are needed to explore

possible dissociation and spin transitions in the (Mg,Fe)O system and the relationship, if any, between them.

4.5.4. SiO_2. The high-pressure behaviour of silica has been extensively studied because of its technological importance and also because it serves as a model system for understanding the octahedrally coordinated silicates of deep planetary interiors. Stishovite, the rutile-structured polymorph of SiO_2, undergoes a displacive transformation to an orthorhombic $CaCl_2$-type structure near 50 GPa [266, 267]. The transformation mechanism as well as the elasticity and strength of SiO_2 across this transition have been examined using synchrotron techniques [114, 116]. Theoretical studies indicate that a large number of structurally related phases of SiO_2 are possible at high pressures and that many of these phases possess similar total energies [268]. Detailed studies of polymorphism in a range of AX_2-type compounds, including oxides such as GeO_2 and SnO_2, provide further insight into the probable sequence of structural changes in silica at high pressures and temperatures [269–272].

There are conflicting reports, at pressures above 75 GPa, about the stability of SiO_2 phases from x-ray diffraction experiments using heated diamond anvil cells. Most studies report the stability of the $CaCl_2$-type form at 120 GPa [267, 273–276], although others have reported the formation of a polymorph related to the α-PbO_2-type structure at pressures of $\sim$80 GPa [277, 278]. More recently, the transformation from the $CaCl_2$-type structure to the α-PbO_2-type structure was reported at 121 GPa and 2400 K, and this new phase was found to be stable at 151 GPa and 2500 K [276]. To further complicate the picture, there have been several reports of formation of, presumably, metastable high-pressure polymorphs at relatively low temperatures using externally heated diamond cells or from different starting materials, such as tridymite [272, 279, 280]. This is not surprising in view of the concept that there are a number of energetically similar phases that can be generated from hexagonally close packed arrays of oxygen with Si cations occupying one-half of the octahedral sites. In such a case, the observed phase in an experiment could depend on starting material, deformation history, temperature, deviatoric stress and heating duration. Identification of the thermodynamically stable phase becomes experimentally challenging and requires a thorough understanding of the response of SiO_2 samples to the above factors. Indeed, a recent study showed that the $CaCl_2$-type phase is observed up to 131 GPa when stishovite starting material is used [275], while α-PbO_2 form can be synthesized at room temperatures from cristobalite starting material at pressures as low as 45 GPa [278]. However, laser heating of α-PbO_2-type SiO_2 formed from cristobalite leads to the formation of the $CaCl_2$-type phase at 79–101 GPa, indicating that the $CaCl_2$-type phase is the thermodynamically stable phase under these conditions [275].

4.6. Post-perovskite phase and the core–mantle boundary

The recent discovery by Murakami *et al* [281] of a transformation from $MgSiO_3$ perovskite to a post-perovskite ($CaIrO_3$-type) phase at $\sim$125 GPa is a major finding that could force drastic reordering of our picture of the structure and dynamics of the core–mantle boundary region. The post-perovskite transformation in $MgSiO_3$ was rapidly confirmed or independently discovered by other experiments and theoretical calculations which also provided additional insight into some physical and thermodynamic properties of the new phase [282–285]. The orthorhombic $CaIrO_3$-type phase consists of edge-sharing chains of SiO_6 octahedra linked by apical oxygens to form sheets along the (010) plane (figure 14). The octahedral sheets are separated into eight-fold coordinated magnesium layers. The structure is anisotropic being more compressible in the *b* direction. The density increase associated with the transition is 0.9–1.2% [281, 286]. Synchrotron diffraction experiments have shown that the presence of iron

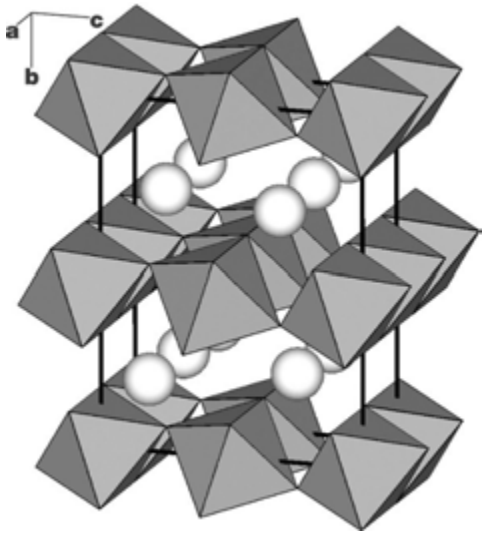

Figure 14. Crystal structure of the $CaIrO_3$-type phase of $MgSiO_3$. SiO_6 octahedron and Mg atoms (spheres) are shown. From [282].

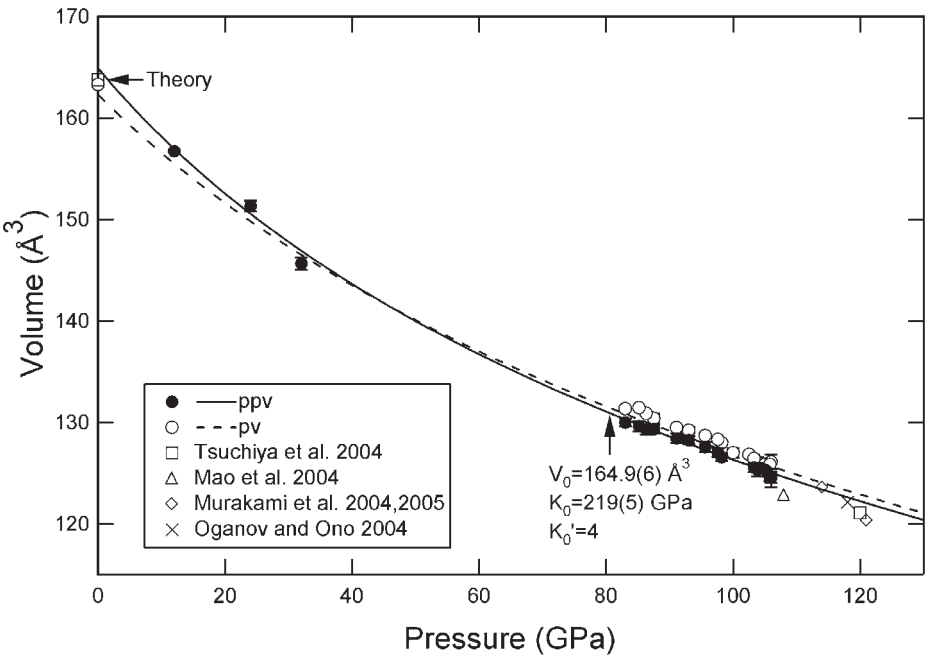

Figure 15. Equations of state of the perovskite and post-perovskite ($CaIrO_3$-type) phases of $(Mg_{0.9}, Fe_{0.1})SiO_3$ [286]. Sources of data: circles and solid line [286]; other experiments (diamond, triangle, dashed line) [230, 246, 281, 287]; theory (square, cross) [282, 283].

may lower the transition boundary in (Mg,Fe)SiO_3 compositions [287]. Room-temperature measurements of Mg#90 samples have constrained the equation of state and the volume change across the phase boundary over a wide pressure range [286] (figure 15). Subsequently, the post-perovskite phase has been identified and characterized in $MgGeO_3$ [288, 289] (figure 10).

The post-perovskite phase transformation also occurs in perovskites formed in natural peridotites and basaltic compositions [224, 246]. In peridotite, the transformation from perovskite to post-perovskite was observed at 113 GPa and 2500 K [246], consistent with the transition pressure observed in an $(Mg_{0.9}, Fe_{0.1})SiO_3$ composition [286]. These conditions correspond to about 400 km above the core–mantle boundary, and thus lie ∼100–200 km above the expected depth of the D″ seismic discontinuity. Chemical analysis of recovered samples shows that Fe–Mg partition coefficient between coexisting ferropericlase and the post-perovskite phase is large, indicating that iron is strongly depleted in the post-perovskite phase compared with the perovskite phase at lower pressures [246]. On the other hand, Mao *et al* [287] suggested that the post-perovskite phase is enriched in iron, on the basis of an analysis of x-ray diffraction data. A strong change in Fe–Mg partitioning in the deep lower mantle may have important geophysical implications as this may affect electrical conductivity, viscosity, melting and heat transport [246]. In basaltic compositions, the phase assemblage identified at 143 GPa and ∼3000 K consisted of an (Mg,Fe)SiO_3 post-perovskite phase, $CaSiO_3$ perovskite, α-PbO_2-type SiO_2 and a $CaTi_2O_4$-type aluminous phase [224].

5. Selected applications of synchrotron research to the core

Iron-rich cores exist in all the terrestrial planets and in many large satellites. The pressures at which cores occur in our solar system span about two orders of magnitude ranging from ∼3 GPa at the top of the core for bodies such as Jupiter's satellite Europa to 363 GPa at the centre of Earth's core. The relative range of temperature encountered in cores spans a likely range of less than a factor of 10. The temperatures of relevance for core physics and chemistry can be, roughly, bounded at one end by the low-pressure Fe–FeS eutectic (∼1250 K at 1 bar), and at the high end by the melting temperature of pure iron near the centre of the Earth (∼6000 K).

The nature of the Earth's core bears on a host of geophysical questions including planet formation and evolution, bulk chemistry of the Earth, magnetic field generation and dynamics, core–mantle interactions and planetary temperature structure. Heat from the core contributes to the driving force for mantle convection. Interest in planetary cores has been stimulated by remote observations and spacecraft exploration of planets that have provided new insights into the state of cores throughout the solar system [290]. For example, Ganymede, the largest satellite in the solar system, was discovered to have an internally generated magnetic field by the Galileo spacecraft [291]. While the P–T conditions of the Earth's solid inner core (330–363 GPa ∼4000–6000 K) still exceed those achievable by direct static experimental investigation, synchrotron studies of the crystal structure, melt properties, equation of state, thermodynamic properties and electronic and magnetic properties of iron and iron alloys over a range of P–T conditions play an integral role in understanding and interpreting geophysical data for planetary cores across the solar system.

5.1. Crystal structure of iron

At low pressures and temperatures, iron has four solid phases: α- and δ-Fe, body centred cubic (bcc) phases that are stable at low P and T and at high T just below the melting point, respectively; γ-Fe, a face centred cubic phase (fcc) stable at high temperatures and ε-Fe, a hexagonal close packed (hcp) phase stable at high pressures and low temperatures. At higher pressures, there have been some reports from diamond anvil cell experiments of the existence of additional phases, including a double hexagonal close packed phase (dhcp) [292–294], and an orthorhombic phase [295, 296]. However, other high-pressure studies

have not observed these phases [93, 106, 297–299]. It is plausible that these polymorphs are metastable and related to temperature or stress gradients in the diamond cell [106, 296, 298]. This conclusion is supported by multi-anvil experiments, under more uniform temperature conditions, that reported no evidence for these phases at conditions now reaching up to 44 GPa and 2100 K [93, 297, 299]. Such conflicting experimental results highlight the complexity and difficulty of high-pressure experiments on even simple systems at extreme conditions.

The possible existence of a high-pressure bcc phase of iron has been considered for many years (e.g. [300]) but no definitive proof has been obtained as yet. Synchrotron x-ray diffraction experiments on Fe have now reached conditions as high as 161 GPa and 3000 K [298]. Only the ε-phase was observed at pressures higher than 60 GPa. Recent *ab initio* molecular dynamics free energy calculations have suggested that a bcc phase could be stabilized at core conditions by the presence of silicon or sulfur impurities [301]. Synchrotron diffraction experiments [302] on Fe–Si alloys have indeed shown that the presence of Si in Fe greatly extends the stability of the bcc phase and it was proposed that the inner core could contain a Si-rich bcc phase and a Si-poor hcp phase.

5.2. Elasticity of iron

Understanding the elastic properties of iron and iron alloys is necessary to resolve structural and compositional issues related to the Earth's core. Some of the central questions are: (1) how do the inner and outer core differ in bulk composition, and what is the corresponding role of chemical versus thermal convection in driving fluid flow in the outer core? (2) Does the low anomalous shear velocity (and corresponding high Poisson's ratio) of the inner core represent the effects of partial melt, anelastic behaviour or the anharmonic elastic response of the core forming material?

In the past, experimental constraints on sound velocities of Fe and Fe alloys have largely been obtained from shock compression [11, 300, 303] as static methods were confined to very low pressures. The advent of new synchrotron-based techniques has now expanded the capabilities of static measurements and broadened our understanding of elastic properties at very high pressures. Using NRIXS techniques, the elastic, thermodynamic and vibrational properties of hcp iron were measured at 153 GPa at room temperature [144, 145]. These measurements have now been extended to simultaneous high pressures and temperatures [121]. Compressional velocities, V_P, determined by IXS have also been reported to more than 100 GPa [134, 140]. Figure 16 shows a compilation of the recent results. Aggregate compressional velocities from NRIXS, IXS and radial x-ray diffraction are in general agreement, and define a linear $V_P - \rho$ trend that lies slightly above shock compression data. 300 K aggregate compressional velocities in pure Fe are consistent with inner core values when extrapolated linearly in density (Birch's law). The experimental data and their extrapolation show some significant differences with theoretical calculations. Shear velocities are derived from IXS or NRIXS experiments by combining compressional or Debye velocity and equation of state data and, therefore, are more uncertain. Also, extrapolations using Birch's law are of uncertain reliability for shear properties. The shear velocity data exhibit more scatter and there is more variance between the trends from different datasets. Nevertheless, extrapolated 300 K shear velocities generally lie well above the inner core values, suggesting the potential importance of phenomena such as chemical impurities, intrinsic (volume independent) anharmonic thermal effects, anelasticity or even partial melting in determining the very low shear velocities in the inner core. It is worth noting that shear velocities inferred from shock data [300, 304] are more consistent with inner core values, suggesting a possible prominent role for anharmonic thermal effects.

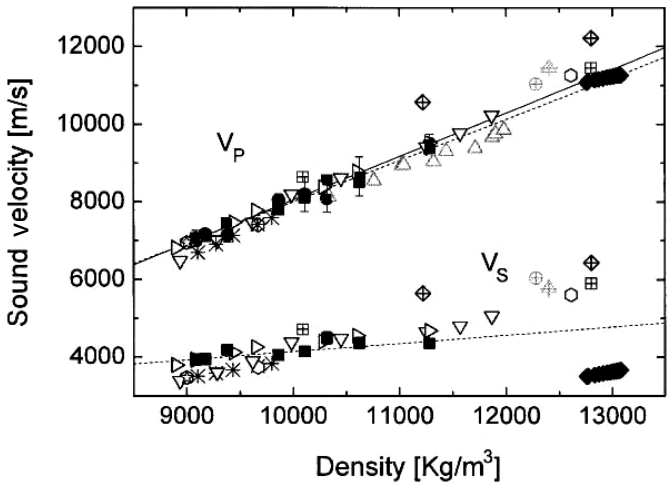

Figure 16. Longitudinal (V_P) and shear (V_S) sound velocities in iron as a function of density. Filled diamonds are seismic data for the inner core. Filled circles and squares—IXS [134, 140], inverted triangles—NRIXS [144], hexagons and asterisks—x-ray diffraction data [58, 358, 359], triangles—shock data [300], crossed symbols—theoretical calculations. From [140].

Another important feature of the Earth's inner core is that it is elastically anisotropic [305]. Seismic waves that travel along polar paths are ∼3% faster than seismic waves that travel along equatorial paths. To explain this observation requires an understanding of the composition, structure, mechanical properties and deformation behaviour of the inner core. Anisotropy of the inner core could result from such phenomena as magnetic field induced preferred orientation, solid-state convection or texturing during solidification.

Radial x-ray diffraction techniques have been used to examine the elastic anisotropy of hcp iron at 211 GPa [58]. A large anisotropy of compressional wave velocity was observed which is at conflict with predictions from theoretical studies [306, 307]. Observed strain anisotropy in radial diffraction may reflect stress variation owing to preferred slip systems. This is supported by radial x-ray diffraction measurements on the polycrystalline hcp metal rhenuim, which showed that the diffraction results were inconsistent with constraints from ultrasonic data [104].

Under non-hydrostatic compression, hcp iron develops a strong fibre texture with the c-axis preferentially aligned along the axis of the diamond cell as a result of basal slip [308, 309]. An IXS study of a textured polycrystal of iron was carried out at 112 GPa [140]. Compressional velocities normal to the c-axis were observed to be 4–5% lower than those 50° away from c, a velocity difference of the same order as the observed inner core anisotropy, suggesting that the degree of alignment in the inner core may be of an order of magnitude comparable to that developed in diamond anvil cell samples.

The full elastic tensor of a single-crystal hcp metal, cobalt, has been investigated at 39 GPa using IXS [310]. Elastic constants could be determined with a precision of a few per cent for the diagonal constants but there are larger uncertainties for off-diagonal terms in the elastic tensor. Such studies require considerable care to avoid destruction of the single crystal, near-hydrostatic and near hydrostatic conditions in the cell are maintained through the use of a helium pressure-transmitting medium. The IXS results show qualitative agreement with the trends from theoretical calculations (at 0 K) using density functional theory [307], but the shape of the acoustic velocity surface does not agree with radial diffraction measurements

on hcp polycrystals [58]. The study of elastic constants by IXS techniques offers greater promise as these measurements can be applied to opaque samples over a wide pressure range. Further, single-crystal studies can help to understand the effect of texturing and anisotropy on geophysical materials.

5.3. Fe–FeS system

Sulfur is a strong candidate light element in planetary cores owing to its solubility in iron, the low eutectic temperatures of the Fe–FeS system and the abundance of iron sulfides in meteorites [311]. The amount of sulfur that could be accreted into a growing Earth may, ultimately, be limited by its high volatility, though this may be a less significant issue for smaller planets and satellites that did not suffer as much accretional heating. Iron sulfide, FeS, exhibits a number of solid phases at high pressures, including a hexagonal NiAs-type phase (phase V) at high temperatures and a phase with a NiAs-type superstructure (phase IV) at intermediate temperatures [312]. Extension of measurements to higher P–T conditions using the laser-heated diamond cell showed that phase V is the stable phase at high temperature and Martian core pressures [103]. Along with extensive polymorphism, FeS possesses a number of interesting complexities associated with its electronic properties. FeS IV exhibits anomalous compression with an abrupt c-axis shortening around 5–9 GPa, which was attributed to an electronic transition of Fe from the high-spin state to a low-spin state [312–314]. Phase V also undergoes an isostructural phase transition at similar pressures and higher temperatures [315]. At room temperature, FeS transforms from the troilite structure to an MnP-related structure at 3.5 GPa and then to a new structure (Phase III) above 6.7 GPa [314,316]. This structure, which is a monoclinic and distorted NiAs-type phase characterized by short Fe–Fe distances, was unknown for a long time but was finally solved using angle-dispersive synchrotron powder diffraction [317]. Synchrotron XES measurements showed that this transformation is also accompanied by a high-spin to low-spin transition in Fe [156]. ^{57}Fe nuclear resonant inelastic scattering was also used to measure the DOSs and derive thermodynamic properties for FeS [318]. Recently, a variety of other probes, including conventional Mossbauer spectroscopy and electrical resistivity [319–321], have also been applied to iron sulfide at pressure. FeS thus provides a striking example of how new or improved synchrotron-based techniques in conjunction with conventional measurements enables us to construct a dramatically improved and integrated picture of crystal structures, electronic properties and physical properties at conditions directly relevant to planetary cores.

While the Fe–S system forms a simple eutectic up to 14 GPa, a number of intermediate compounds (Fe_3S_2, Fe_2S and Fe_3S) have been found at higher pressures and some of their equations of state, structures and elastic properties have been investigated by synchrotron techniques [322,323]. Fe_3S was studied using NRIXS and SMS at 57 GPa at room temperature. A magnetic transition was observed at 21 GPa, which affects the sound velocities [151]. Fe_3C, another candidate core material, also undergoes a magnetic transition near 25 GPa, as found in an XES study [161].

5.4. Melting of iron

The melting curve of iron remains controversial. Early studies were based on either visual observations of melt in the laser-heated diamond cell or on measurements of temperatures resulting from shock compression. However, these methods produced conflicting melting curves that differed by as much as 1200 K at 100 GPa [324, 325] (figure 17). Since then, there have been numerous additional studies using a variety of experimental and theoretical

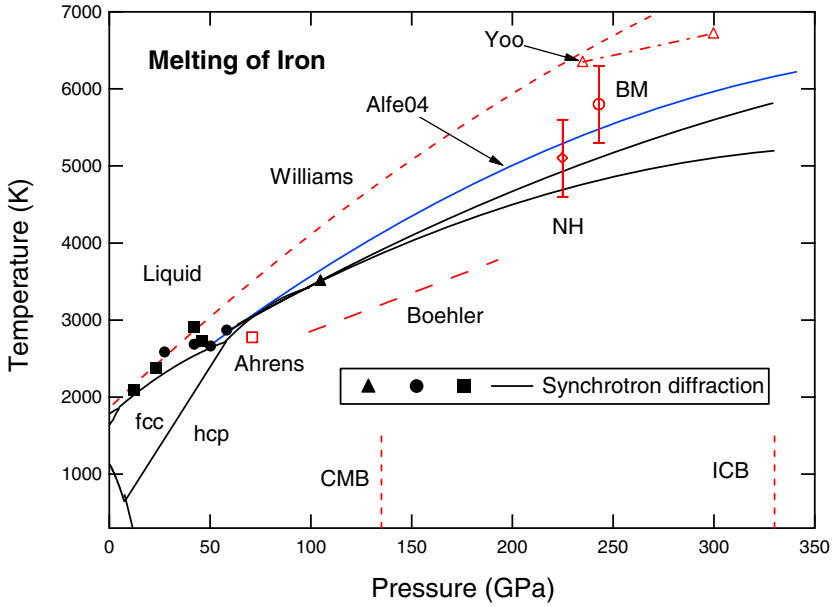

Figure 17. Phase diagram and melting curve of iron. The solid black symbols are melt observations from synchrotron diffraction experiments [106, 121, 298] and the solid black lines show phase boundaries and melting curve consistent with these results and extrapolated to higher pressures [298]. Other constraints on the melting line are from theory ($AlFeO_4$) [328], shock compression (NH, BM, Yoo, Ahrens) [300, 324, 331, 334, 335] and static compression with visual observations (Williams, Boehler) [324, 325]. fcc—face centred cubic phase (γ) and hcp—hexagonal close packed phase (ε). ICB = inner core boundary and CMB = core–mantle boundary.

methods and melting criteria, and only recently has something approaching a consensus emerged.

Theoretical studies using density functional theory have been used to calculate melting curves of Fe using either Gibbs free energy calculations for the solid and liquid or a method of solid/liquid coexistence, which uses model potentials fit to quantum mechanical calculation results [326–330]. Initial results showed large discrepancies between methods. Further examination has led to modifications and corrections and these appear to be able to explain much of the discrepancy [327, 328]. A theoretical melting curve of iron consistent with both the Gibbs free energy method and model potential calculations is shown in figure 17 [328].

Shock compression studies that involve measured shock temperatures, using either gas guns or laser shocks, generally yield melting temperatures for Fe at the high end of the experimental range [324, 331, 332]. This could be associated with superheating along the shock Hugoniot curve [333] or systematic errors in temperature measurements. Initially, sound velocity measurements along the Hugoniot indicated that melting occurs at 243 GPa [300], but a more recent study puts the melting velocity discontinuity at 225 GPa [334]. Thermodynamically calculated temperatures at these pressures are 5800 ± 500 K [300] and 5100 ± 500 K [334], respectively. These are well below the results for direct measurements of shock temperatures. Another recent study using preheated iron samples determined that melting occurs near 71 GPa and 2771 K along this high-temperature Hugoniot path [335].

Shen *et al* [106] used energy dispersive synchrotron diffraction experiments to place constraints on the melting curve to 84 GPa. A later study, using similar techniques, extended

melting determination at 105 GPa and 3510 K [298]. However, measurements of melting using a point detector can be biased owing to the limited azimuthal coverage of the diffracted cone. Recently, angle dispersive measurements using diffuse scattering from the melt as a positive melting criterion have been reported [121] and these are in agreement with the previous energy-dispersive data.

Figure 17 summarizes constraints on the melting curve of iron. Phase boundaries to 100 GPa are based on synchrotron x-ray diffraction results [106, 121, 298]. These are consistent with the latest improved theoretical calculations [328] and calculated shock temperatures at the melting pressured at 225 GPa, obtained from recent Hugoniot sound velocity measurements [334]. This convergence of recent results from static experiment, shock compression and theory suggests that a consensus on the melting curve of Fe may be developing. However, the melting curve of Boehler, based on visual observations, lies at significantly lower temperatures and the discrepancy amounts to about 600 K (or ∼20%) at 105 GPa [325].

Extrapolation of the synchrotron-based melting curve yields melting temperatures for Fe at the inner core boundary of 5200–5900 K, whereas theoretical calculations yield a value near 6300 K [328]. Extrapolating the range from synchrotron experiments along a plausible core geotherm [13] yields estimated temperatures of 3600–4400 K at the core–mantle boundary. The temperature at the inner core boundary, however, may differ from that of pure Fe because of freezing point depression owing to the presence of a light element. Thus, the melting behaviour must also be constrained in more complex systems [70]. While the exact change in the melting point will depend on the identity of the light element(s), existing estimates suggest that the effect will be ∼500–1000 K at core pressures [70].

5.5. Properties of iron and iron-alloy liquids

Planetary cores, even those of some satellites and small planets (e.g. Io, Mars) without detectable internal magnetic fields, are likely to have, at least partially, liquid interiors even up to the present day [290]. The study of the properties of liquids in the Fe–FeS system has also benefited from synchrotron developments including measurements of liquid densities and viscosities using x-ray absorption profiles or x-ray radiography combined with falling sphere viscometry, as outlined earlier. Densities of liquids in the Fe–S and Fe–Si system were measured up to 5–6 GPa at temperatures above 1700 K [336, 337]. The results by this method are broadly consistent with density bounds inferred from sink/float experiments up to 20 GPa [338]. The addition of sulfur strongly reduces the density (and increases the compressibility) of the melt.

The viscosity of iron and iron-alloys are one of the fundamental parameters needed to characterize convective flow and operation of the geodynamo in the Earth's outer core. Measurements of the viscosity of Fe–FeS compositions to 7 GPa using Stokes' viscometry yield viscosities of $\sim 10^{-2}$ Pa s [339–342] and an estimated viscosity of 2×10^{-2} Pa s for the Earth's outer core was reported [340]. The viscosity of pure Fe liquid has also been measured up to ∼6 GPa and 2100 K in two studies [340, 343], though they show some disagreement in the pressure dependence of viscosity and its relation to melt structure [344].

Macroscopic properties, such as viscosity, depend on the nature of the local structure of the liquid. Synchrotron x-ray diffraction on liquid iron has been used to determine the radial distribution function at 5 GPa and 2300 K [344]. As pressure increases, a bcc-like structure in liquid iron evolves towards a more close-packed structure. More recently, the structure of liquid iron was examined in the diamond anvil cell at 58 GPa using angle dispersive diffraction techniques [121] demonstrating that liquid iron behaves as a close-packed hard-sphere liquid.

Theoretical calculations [345] suggest that iron remains a relatively simple close-packed liquid even at core conditions, and the viscosity is similar to values at ambient pressure. X-ray diffraction studies to constrain the radial distribution functions of Fe–S and Fe–Si liquids were carried out up to 5 GPa and 1400–2300 K in a large-volume apparatus [346]. Si produces little change in melt structure compared with pure Fe, but the presence of S strongly modifies the local structure. This result is consistent with the observed large effect of sulfur on melt compressibility obtained by the x-ray absorption method discussed earlier.

6. Experimental challenges

Synchrotron experiments directed at understanding planetary interiors have experienced considerable evolution in recent years. There are a number of areas of experimental challenge where future advancements may develop.

Although improvements in pressure and temperature metrology can enhance all types of high-pressure synchrotron experiments, they are especially needed for understanding mantle phase transitions. Progress has been made in developing better high P–T equation of state standards [52, 181, 184], and increasingly extensive cross-calibrations have been carried out [54]. Further efforts are needed to improve calibration of standards at very high pressures exceeding 1 Mbar [49]. P–V–T equations of state used at present involve a number of simplifying assumptions, and more sophisticated formuations need to be developed. Theoretical studies using density functional theory should play a greater role in constraining the form of the equation of state and the higher order thermodynamic parameters that are often required. Absolute pressure scales can be constructed from acoustic and volume compression data [47, 48] while careful, detailed studies are needed at high P–T to establish well-characterized absolute standards.

There have also been significant strides in temperature generation and measurement capabilities in different high-pressure apparatus. The use of intensity ratios of phonon creation and annihilation (Stokes/anti-Stokes) pairs, from Raman [347] or nuclear resonance spectroscopy [84] for absolute temperature determination, is a significant development with the potential to resolve long-standing uncertainties associated with spectroradiometry. In large-volume apparatus, thermal noise metrology offers a possible route to an absolute calibration if measurements of sufficient accuracy can be extracted from the weak Johnson noise signal.

High-pressure technology promises to continue to evolve, expanding the P–T range and experimental accuracy of existing techniques while also making entirely new measurements possible. For the diamond anvil cell, synthetic single-crystal diamond grown by chemical vapour deposition (CVD) techniques have been developed for ultra-high pressures [348]. Growth of CVD layers on natural diamonds allows for various probes to be encapsulated within diamond, thereby creating new opportunities for electrical and magnetic measurements, heating systems and isotopic control of diamond composition [349]. Supported Moissanite (SiC) cells have been developed that allow for significant increases in sample volume [350]. In the multi-anvil apparatus, the use of sintered diamond anvils not only allows for pressure generation up to 60 GPa or above [351] but also provides an optical window that can enable new types of high-pressure experiments [92].

Nuclear resonant and inelastic scattering techniques have just begun to be exploited at high pressures as they have considerable potential application to geophysical problems. These are count-rate limited experiments, and further improvements in photon flux and stability of laser heating are expected in the future.

Development of monochromatic single-crystal diffraction techniques at the megabar pressure range promises to be a frontier research direction for diamond anvil cell studies

over the next decade. There are a number of requirements for such experiments that are being actively addressed, including hydrostaticity of the pressure environment, size and integrity of the single crystal at very high pressures, access to a sufficient portion of reciprocal space and a diffraction system for accurate intensity and d-spacing measurement. Development of new diamond cell designs, x-ray transparent gaskets and new types of x-ray transparent backing plates are also integral parts of this effort.

7. Summary

Synchrotron-based high-pressure experiments have contributed greatly to our understanding of material properties at high pressures and to our ability to interpret geophysical observations of the deep Earth and planetary interiors. The last few years have witnessed rapid, synergistic development of advanced pressure-generating capabilities and new synchrotron techniques. At the same time, more established techniques, such as x-ray diffraction, witness continual improvements in quality and capability. Examples of the most significant findings over the last five years include the following:

(1) The discovery and characterization of the post-perovskite ($CaIrO_3$-type) phase of $MgSiO_3$ at pressures near 125 GPa. The existence of a first-order phase change in the most abundant mantle constituent promises to have a major impact on our understanding of core–mantle boundary dynamics.
(2) Development of high-pressure inelastic scattering and spectroscopic techniques which have enabled many electronic, magnetic and vibrational properties to be characterized directly at high pressure for the first time. Examples include the discovery of spin pairing transitions in Fe alloys and Fe-bearing silicates under deep Earth conditions.
(3) Synchrotron x-ray diffraction techniques in both the diamond anvil cell and multi-anvil apparatus have allowed for detailed examination of the depth, slope, thickness and velocity contrast of the major upper mantle seismic discontinuities under *in situ* conditions for the first time.
(4) The study of melting, melt structure and physical properties of melts as well as liquids using a variety of diffraction and spectroscopic techniques. Understanding of the behaviour of melts at very high-pressure conditions is critical to understanding Earth formation and evolution as well as core structure and its dynamics.
(5) The study of the strength and rheology of silicates across the upper mantle P–T range and at deep mantle pressures at room temperatures. Ultimately, rheological properties ultimately control mantle flow, but until recently it had been among the more poorly constrained physical properties of minerals.

Acknowledgments

The manuscript benefited by comments from A Kubo. S-H Shim, A Kubo, S Speziale and S Shieh provided assistance in the preparation of the figures. The NSF, DOE and David and Lucile Packard Foundation provided financial support.

References

[1] Kennett B L N, Engdahl E R and Buland R 1995 *Geophys. J. Int.* **122** 108–24
[2] Garnero E J 2000 *Ann. Rev. Earth Planet. Sci.* **28** 509–37
[3] Sidorin I, Gurnis M and Helmberger D V 1999 *Science* **286** 1326–31
[4] Lay T and Helmberger D V 1983 *Geophys. J. R. Astron. Soc.* **75** 799–837

[5] Williams Q and Garnero E J 1996 *Science* **273** 1528–30
[6] Christensen U R and Hofmann A W 1994 *J. Geophys. Res.* **99** 19867–84
[7] Romanowicz B 1991 *Ann. Rev. Earth Planet. Sci.* **19** 77–99
[8] van der Hilst R D, Widiyantoro S and Engdahl E R 1997 *Nature* **386** 578–84
[9] Montelli R, Nolet G, Dahlen F A, Masters G, Engdahl E R and Hung S H 2004 *Science* **303** 338–43
[10] van Keken P E, Hauri E H and Ballentine C J 2002 *Ann. Rev. Earth Planet. Sci.* **30** 493–525
[11] Duffy T S and Ahrens T J 1992 *J. Geophys. Res.* **97** 4503–20
[12] Karato S-I and Karki B B 2001 *J. Geophys. Res.* **106** 21771–83
[13] Stixrude L and Brown J M 1998 *Ultrahigh-Pressure Mineralogy* ed R J Hemley (Washington, DC: Mineralogical Society of America) pp 261–82
[14] Jephcoat A and Olson P 1987 *Nature* **325** 332–5
[15] Buffett B A, Huppert H E, Lister J R and Woods A W 1996 *J. Geophys. Res.* **101** 7989–8006
[16] Stevenson D J 2001 *High-Pressure Phenomena* ed G L Chiarotti *et al* (Amsterdam: IOS) pp 587–606
[17] McCammon C 2001 *Science* **293** 813–14
[18] McDonough W F and Sun S S 1995 *Chem. Geol.* **120** 223–53
[19] Fei Y and Bertka C M 1999 *Mantle Petrology: Field Observations and High Pressure Experiments* ed Y Fei *et al* (Houston: The Geochemical Society) pp 189–207
[20] Helffrich G R and Wood B J 2001 *Nature* **412** 501–7
[21] Duffy T S, Zha C S, Downs R T, Mao H-k and Hemley R J 1995 *Nature* **378** 170–3
[22] Katsura T *et al* 2004 *J. Geophys. Res.* **109** B02209
[23] Hacker B R, Abers G A and Peacock S M 2003 *J. Geophys. Res.* **108** 2029
[24] Tackley P J, Stevenson D J, Glatzmaier G A and Schubert G 1994 *J. Geophys. Res.* **99** 15877–901
[25] Christensen U 1995 *Ann. Rev. Earth Planet. Sci.* **23** 65–87
[26] Weidner D J, Chen J H, Xu Y Q, Wu Y J, Vaughan M T and Li L 2001 *Phys. Earth Planet. Int.* **127** 67–81
[27] Weidner D J 1998 *Rev. Mineral.* **37** 493–524
[28] Durham W B, Weidner D J, Karato S I and Wang Y B 2002 *Plastic Deformation of Minerals and Rocks* ed S Karato and H R Wenk (Washington, DC: Mineralogical Society of America) pp 21–49
[29] Kellogg L H, Hager B H and van der Hilst R D 1999 *Science* **283** 1881–4
[30] van der Hilst R D and Karason H 1999 *Science* **283** 1885–8
[31] Ishii M and Tromp J 1999 *Science* **285** 1231–6
[32] Kennett B L N, Widiyantoro S and van der Hilst R D 1998 *J. Geophys. Res.* **103** 12469–93
[33] Williams Q and Hemley R J 2001 *Ann. Rev. Earth Planet. Sci.* **29** 365–418
[34] Yusa H, Inoue T and Ohishi Y 2000 *Geophys. Res. Lett.* **27** 413–16
[35] Chen J, Inoue T, Weidner D J, Wu Y and Vaughan M T 1998 *Geophys. Res. Lett.* **25** 575–8
[36] Kavner A 2003 *Earth Planet. Sci. Lett.* **214** 645–54
[37] Song T R A, Helmberger D V and Grand S P 2004 *Nature* **427** 530–3
[38] van der Meijde M, Marone F, Giardini D and van der Lee S 2003 *Science* **300** 1556–8
[39] Nolet G and Zielhuis A 1994 *J. Geophys. Res.* **99** 15813–20
[40] Hemley R J, Mao H-k and Struzhkin V V 2005 *J. Synch. Rad.* **12** 135–54
[41] Paszkowicz W 2002 *Nucl. Instrum. Methods* B **198** 142–82
[42] Singh A K 1993 *J. Appl. Phys.* **73** 4278–86
[43] Duffy T S, Hemley R J and Mao H-k 1995 *Phys. Rev. Lett.* **74** 1371–4
[44] Piermarini G J, Block S, Barnett J D and Forman R A 1975 *J. Appl. Phys.* **46** 2774–80
[45] Mao H K, Bell P M, Shaner J W and Steinberg D J 1978 *J. Appl. Phys.* **49** 3276–83
[46] Mao H K, Xu J and Bell P M 1986 *J. Geophys. Res.* **91** 4673–6
[47] Zha C S, Mao H-k and Hemley R J 2000 *Proc. Natl Acad. Sci.* **97** 13494–9
[48] Zha C S, Duffy T S, Downs R T, Mao H-k and Hemley R J 1998 *Earth Planet. Sci. Lett.* **159** 25–34
[49] Dewaele A, Loubeyre P and Mezouar M 2004 *Phys. Rev.* B **70** 094112
[50] Funamori N and Jeanloz R 1997 *Science* **278** 1109–11
[51] Lin J F, Degtyareva O, Prewitt C T, Dera P, Sata N, Gregoryanz E, Mao H K and Hemley R J 2004 *Nat. Mat.* **3** 389–93
[52] Holzapfel W B 2003 *J. Appl. Phys.* **93** 1813–18
[53] Dorogokupets P I and Oganov A R 2003 *Dokl. Earth Sci.* A **391** 854–7
[54] Fei Y W, Li H, Hirose K, Minarik W, Van Orman J, Sanloup C, van Westrenen W, Komabayashi T and Funakoshi K 2004 *Phys. Earth Planet. Int.* **143–144** 515–26
[55] Mao H K, Kao C C and Hemley R J 2001 *J. Phys.: Condens. Matter* **13** 7847–58
[56] Yamanaka T, Fukuda T, Hattori T and Sumiya H 2001 *Rev. Sci. Instrum.* **72** 1458–62

[57] Mao H K, Shen G, Hemley R J and Duffy T S 1998 *High-Pressure Temperature Research: Properties of Earth and Planetary Materials* ed M H Manghnani and T Yagi (Washington, DC: American Geophysical Union) pp 27–34
[58] Mao H K, Shu J F, Shen G, Hemley R J, Li B and Singh A K 1998 *Nature* **396** 741–3
[59] Hemley R J, Mao H-k, Shen G, Badro J, Gillet P, Hanfland M and Hausermann D 1997 *Science* **276** 1242–5
[60] Lin J F, Shu J, Mao H K, Hemley R J and Shen G 2003 *Rev. Sci. Instrum.* **74** 4732–6
[61] Fei Y and Wang Y 2000 *Rev. Mineral. Geochem.* **41** 551–7
[62] Zha C S and Bassett W A 2003 *Rev. Sci. Instrum.* **74** 1255–62
[63] Dubrovinskaia N and Dubrovinsky L 2003 *Rev. Sci. Instrum.* **74** 3433–7
[64] Jephcoat A P and Besedin S P 1996 *Phil. Trans. R. Soc. Lond.* A **354** 1333–60
[65] Ming L and Bassett W A 1974 *Rev. Sci. Instrum.* **45** 1115–18
[66] Shen G, Rivers M L, Wang Y and Sutton S R 2001 *Rev. Sci. Instrum.* **72** 1273–82
[67] Lin J F, Sturhahn W, Zhao J, Shen G, Mao H-k and Hemley R J 2005 *Advances in High-Pressure Technology for Geophysical Applications* ed J Chen *et al* (Amerstdam: Elsevier) at press
[68] Watanuki T, Shimomura O, Yagi T, Kondo T and Isshiki M 2001 *Rev. Sci. Instrum.* **72** 1289–92
[69] Yagi T, Kondo T, Watanuki T, Shimomura O and Kikegawa T 2001 *Rev. Sci. Instrum.* **72** 1293–7
[70] Boehler R 2000 *Rev. Geophys.* **38** 221–45
[71] Andrault D and Fiquet G 2001 *Rev. Sci. Instrum.* **72** 1283–8
[72] Dewaele A, Fiquet G and Gillet P 1998 *Rev. Sci. Instrum.* **69** 2421–6
[73] Kavner A and Panero W R 2004 *Phys. Earth Planet. Int.* **143–144** 527–39
[74] Panero W R and Jeanloz R 2001 *J. Geophys. Res.* **106** 6493–8
[75] Panero W R and Jeanloz R 2001 *Rev. Sci. Instrum.* **72** 1306–8
[76] Kiefer B and Duffy T S 2005 *J. Appl. Phys.* at press
[77] Andrault D, Fiquet G, Itie J P, Richet P, Gillet P, Hausermann D and Hanfland M 1998 *Eur. J. Mineral.* **10** 931–40
[78] Kavner A and Duffy T S 2001 *J. Appl. Phys.* **89** 1907–14
[79] Prakapenka V B, Shen G Y and Dubrovinsky L S 2003 *High Temp.—High Pressures* **35–36** 237–49
[80] Walter M J and Koga K T 2004 *Phys. Earth Planet. Int.* **143–144** 541–58
[81] Eng P J, Newville M, Rivers M L and Sutton S R 1998 *SPIE Proc.* **3449** 145–56
[82] Getting I C and Kennedy G C 1970 *J. Appl. Phys.* **41** 4552
[83] Irifune T 2002 *Mineral. Mag.* **66** 769–90
[84] Lin J F, Sturhahn W, Zhao J Y, Shen G Y, Mao H K and Hemley R J 2004 *Geophys. Res. Lett.* **31** L14611
[85] Zhao J, Sturhahn W, Lin J F, Shen G, Alp E E and Mao H-k 2004 *High Pressure Res.* **24** 447–57
[86] Li B S, Kung J and Liebermann R C 2004 *Phys. Earth Planet. Int.* **143–144** 559–74
[87] Duffy T S and Wang Y 1998 *Ultrahigh Pressure Mineralogy* ed R J Hemley (Washington, DC: Mineralogical Society of America) pp 425–58
[88] Katayama Y and Inamura Y 2003 *J. Phys.: Condens. Matter* **15** S343–S350
[89] Utsumi W, Funakoshi K, Katayama Y, Yamakata M, Okada T and Shimomura O 2002 *J. Phys.: Condens. Matter* **14** 10497–504
[90] Uchida T *et al* 2002 *J. Phys.: Condens. Matter* **14** 11517–23
[91] Besson J M, Nelmes R J, Hamel G, Loveday J S, Weill G and Hull S 1992 *Physica* B **180** 907–10
[92] Katsura T, Funakoshi K, Kubo A, Nishiyama N, Tange Y, Sueda Y, Kubo T and Utsumi W 2004 *Phys. Earth Planet. Int.* **143–144** 497–506
[93] Kubo A, Ito E, Katsura T, Shinmei T, Yamada H, Nishikawa O, Song M S and Funakoshi K 2003 *Geophys. Res. Lett.* **30** 1126
[94] Parise J B, Weidner D J, Chen J, Liebermann R C and Chen G 1998 *Ann. Rev. Mater. Sci.* **28** 349–74
[95] Buras B and Gerward L 1989 *Prog. Cryst. Growth Charact. Mater.* **18** 93–138
[96] Fei Y, Mao H K, Shu J, Parthasarathy G and Bassett W A 1992 *J. Geophys. Res.* **97** 4489–95
[97] Fei Y, Mao H K, Shu J F and Hu J 1992 *Phys. Chem. Minerals* **18** 416–22
[98] Fei Y and Mao H-k 1993 *J. Geophys. Res.* **98** 11875–84
[99] Fiquet G, Andrault D, Itie J P, Gillet P and Richet P 1996 *Phys. Earth Planet. Int.* **95** 1–17
[100] Kruger M B, Nguyen J H, Caldwell W and Jeanloz R 1997 *Phys. Rev.* B **56** 1–4
[101] Shim S-H, Duffy T S and Shen G 2000 *J. Geophys. Res.* **105** 25955–68
[102] Meade C, Mao H K and Hu J 1995 *Science* **268** 1743–5
[103] Kavner A, Duffy T S and Shen G 2001 *Earth Planet. Sci. Lett.* **185** 25–33
[104] Duffy T S, Shen G, Heinz D L, Shu J F, Ma Y, Mao H-k, Hemley R J and Singh A K 1999 *Phys. Rev.* B **60** 15063–73
[105] Shieh S R, Duffy T S and Shen G 2004 *Phys. Earth Planet. Int.* **143–144** 93–106

[106] Shen G, Mao H-k, Hemley R J, Duffy T S and Rivers M L 1998 *Geophys. Res. Lett.* **25** 373–6
[107] Shim S-H, Jeanloz R and Duffy T S 2002 *Geophys. Res. Lett.* **29** 2466
[108] Wenk H R, Lonardelli I, Pehl J, Devine J, Prakapenka V, Shen G and Mao H K 2004 *Earth Planet. Sci. Lett.* **226** 507–19
[109] Chen J H, Weidner D J, Parise J B, Vaughan M T and Raterron P 2001 *Phys. Rev. Lett.* **86** 4072–5
[110] Wang Y B, Uchida T, Von Dreele R, Rivers M L, Nishiyama N, Funakoshi K, Nozawa A and Kaneko H 2004 *J. Appl. Cryst.* **37** 947–56
[111] Mao H K, Jephcoat A P, Hemley R J, Finger L W, Zha C S, Hazen R M and Cox D E 1988 *Science* **239** 1131–4
[112] Shu J F, Mao H K, Hu J Z, Fei Y W and Hemley R J 1998 *N. Jahr. Mineral.* **172** 309–23
[113] Duffy T S, Shu J, Mao H-k and Hemley R J 1995 *Phys. Chem. Minerals* **22** 277–81
[114] Hemley R J, Shu J, Carpenter M A, Hu J, Mao H-k and Kingma K J 2000 *Solid State Commun.* **114** 527–32
[115] Karki B B, Stixrude L and Crain J 1997 *Geophys. Res. Lett.* **24** 3269–72
[116] Shieh S R, Duffy T S and Li B S 2002 *Phys. Rev. Lett.* **89** 25507
[117] Sobolev N V, Fursenko B A, Goryainov S V, Shu J F, Hemley R J, Mao H K and Boyd F R 2000 *Proc. Natl Acad. Sci.* **97** 11875–9
[118] Dera P, Prewitt C T, Boctor N Z and Hemley R J 2002 *Am. Mineral.* **87** 1018–23
[119] Duffy T S and Ahrens T J 1992 *High-Pressure Research in Mineral Physics: Applications to Earth and Planetary Sciences* ed Y Syono and M H Manghnani (Tokyo: Terra Scientific) pp 197–206
[120] Yaoita K, Katayama Y, Tsuji K, Kikegawa T and Shimomura O 1997 *Rev. Sci. Instrum.* **68** 2106–10
[121] Shen G Y, Prakapenka V B, Rivers M L and Sutton S R 2004 *Phys. Rev. Lett.* **92** 185701
[122] Shen G Y, Rivers M L, Sutton S R, Sata N, Prakapenka V B, Oxley J and Suslick K S 2004 *Phys. Earth Planet. Int.* **143–144** 481–95
[123] Funamori N, Yamamoto S, Yagi T and Kikegawa T 2004 *J. Geophys. Res.* **109** B03203
[124] Katayama Y and Tsuji K 2003 *J. Phys.: Condens. Matter* **15** 6085–103
[125] Katayama Y, Tsuji K, Chen J, Koyama N, Kikegawa T, Yaoita K and Shimomura O 1993 *J. Non-Cryst. Solids* **156** 687–90
[126] Shen G Y, Sata N, Newville M, Rivers M L and Sutton S R 2002 *Appl. Phys. Lett.* **81** 1411–13
[127] Scarfe C M, Mysen B O and Virgo D 1987 *Magmatic Processes: Physiochemical Principles* ed B O Mysen (University Park, PA: Geochemical Society) pp 59–68
[128] Kushiro I 1976 *J. Geophys. Res.* **81** 6347–50
[129] Kanzaki M, Kurita K, Fujii T, Kato T, Shimomura O and Akimoto S 1987 *High-Pressure Research in Mineral Physics* ed M H Manghnani and Y Syono (Washington, DC: American Geophysical Union) pp 195–200
[130] Reid J E, Suzuki A, Funakoshi K I, Terasaki H, Poe B T, Rubie D C and Ohtani E 2003 *Phys. Earth Planet. Int.* **139** 45–54
[131] Suzuki A, Ohtani E, Funakoshi K, Terasaki H and Kubo T 2002 *Phys. Chem. Mineral.* **29** 159–65
[132] Tinker D, Lesher C E, Baxter G M, Uchida T and Wang Y B 2004 *Am. Mineral.* **89** 1701–8
[133] Burkel E 2000 *Rep. Prog. Phys.* **63** 171–232
[134] Fiquet G *et al* 2004 *Phys. Earth Planet. Int.* **143–144** 5–18
[135] Occelli F, Krisch M, Loubeyre P, Sette F, Le Toullec R, Masciovecchio C and Rueff J P 2001 *Phys. Rev.* B **63** 224306
[136] Krisch M 2003 *J. Raman Spectrosc.* **34** 628–32
[137] Isaak D G 2001 *Handbook of Elastic Properties of Solids, Liquids, and Gases* ed M Levy *et al* (San Diego: Academic) pp 325–77
[138] Li B S, Liebermann R C and Weidner D J 2001 *J. Geophys. Res.* **106** 30579–91
[139] Krisch M H, Mermet A, SanMiguel A, Sette F, Masciovecchio C, Ruocco G and Verbeni R 1997 *Phys. Rev.* B **56** 8691–4
[140] Antonangeli D, Occelli F, Requardt H, Badro J, Fiquet G and Krisch M 2004 *Earth Planet. Sci. Lett.* **225** 243–51
[141] Antonangeli D, Krisch M, Fiquet G, Farber D, Aracne C, Badro J, Occelli F and Requardt H 2005 *Phys. Rev. Lett.* **93** 215505
[142] Sturhahn W, Toellner T S, Alp E E, Zhang X, Ando M, Yoda Y, Kikuta S, Seto M, Kimball C W and Dabrowski B 1995 *Phys. Rev. Lett.* **74** 3832–5
[143] Sturhahn W 2004 *J. Phys.: Condens. Matter* **16** S497–530
[144] Mao H K *et al* 2001 *Science* **292** 914–16
[145] Lubbers R, Grunsteudel H F, Chumakov A I and Wortmann G 2000 *Science* **287** 1250–3
[146] Shen G, Sturhahn W, Alp E E, Zhao J, Toellner T S, Prakapenka V B, Meng Y and Mao H R 2004 *Phys. Chem. Mineral.* **31** 353–9

[147] Struzhkin V V, Mao H K, Mao W L, Hemley R J, Sturhahn W, Alp E E, L'Abbe C, Hu M Y and Errandonea D 2004 *Hyperfine Int.* **153** 3–15
[148] Hu M Y, Sturhahn W, Toellner T S, Mannheim P D, Brown D E, Zhao J Y and Alp E E 2003 *Phys. Rev.* B **67** 094304
[149] Lin J F, Struzhkin V V, Sturhahn W, Huang E, Zhao J Y, Hu M Y, Alp E E, Mao H K, Boctor N and Hemley R J 2003 *Geophys. Res. Lett.* **30** 2112
[150] Mao W L, Sturhahn W, Heinz D L, Mao H K, Shu J F and Hemley R J 2004 *Geophys. Res. Lett.* **31** L15618
[151] Lin J F, Fei Y W, Sturhahn W, Zhao J Y, Mao H K and Hemley R J 2004 *Earth Planet. Sci. Lett.* **226** 33–40
[152] Jackson J M, Sturhahn W, Shen G Y, Zhao J Y, Hu M Y, Errandonea D, Bass J D and Fei Y W 2005 *Am. Mineral.* **90** 199–205
[153] Zhang L, Stanek J, Hafner S S, Ahsbahs H, Grunsteudel H F, Metge J and Ruffer R 1999 *Am. Mineral.* **84** 447–53
[154] Lin J F, Sturhahn W, Zhao J, Shen G, Mao H-k and Hemley R J 2005 *Advances in High-Pressure Technology for Geophysical Applications* ed J Chen *et al* (Amerstdam: Elsevier) at press
[155] Badro J, Rueff J P, Vanko G, Monaco G, Fiquet G and Guyot F 2004 *Science* **305** 383–6
[156] Rueff J P, Kao C C, Struzhkin V V, Badro J, Shu J, Hemley R J and Hao H K 1999 *Phys. Rev. Lett.* **82** 3284–7
[157] Badro J, Struzhkin V V, Shu J F, Hemley R J, Mao H K, Kao C C, Rueff J P and Shen G Y 1999 *Phys. Rev. Lett.* **83** 4101–4
[158] Badro J, Fiquet G, Struzhkin V V, Somayazulu M, Mao H K, Shen G and Le Bihan T 2002 *Phys. Rev. Lett.* **89** 205504
[159] Badro J, Fiquet G, Guyot F, Rueff J P, Struzhkin V V, Vanko G and Monaco G 2003 *Science* **300** 789–91
[160] Li J, Struzhkin V V, Mao H K, Shu J F, Hemley R J, Fei Y W, Mysen B, Dera P, Prakapenka V and Shen G Y 2004 *Proc. Natl Acad. Sci.* **101** 14027–30
[161] Lin J F, Struzhkin V V, Mao H K, Hemley R J, Chow P, Hu M Y and Li J 2004 *Phys. Rev.* B **70** 212405
[162] Rueff J P, Krisch M, Cai Y Q, Kaprolat A, Hanfland M, Lorenzen M, Masciovecchio C, Verbeni R and Sette F 1999 *Phys. Rev.* B **60** 14510–12
[163] Shinoda K, Yamakata M, Nanba T, Kimura H, Moriwaki T, Kondo Y, Kawamoto T, Niimi N, Miyoshi N and Aikawa N 2002 *Phys. Chem. Mineral.* **29** 396–402
[164] Liu Z X, Lager G A, Hemley R J and Ross N L 2003 *Am. Mineral.* **88** 1412–15
[165] Hemley R J, Goncharov A F, Lu R, Struzhkin V V, Li M and Mao H K 1998 *Nuovo Cim.* D **20** 539–51
[166] Liu Z, Hu J, Yang H, Mao H K and Hemley R J 2002 *J. Phys.: Condens. Matter* **14** 10641–6
[167] Birch F 1952 *J. Geophys. Res.* **57** 227–86
[168] Knittle E 1995 *A Handbook of Physical Constants* ed T J Ahrens (Washington, DC: American Geophysical Union) pp 98–143
[169] Jackson I and Rigden S M 1996 *Phys. Earth Planet. Int.* **96** 85–112
[170] Shim S-H and Duffy T S 2000 *Am. Mineral.* **85** 354–63
[171] Ito E and Takahashi E 1989 *J. Geophys. Res.* **94** 10637–46
[172] Irifune T *et al* 1998 *Science* **279** 1698–700
[173] Hirose K, Fei Y W, Ono S, Yagi T and Funakoshi K 2001 *Earth Planet. Sci. Lett.* **184** 567–73
[174] Walter M J, Thibault Y, Wei K and Luth R W 1995 *Can. J. Phys.* **73** 273–86
[175] Katsura T *et al* 2003 *Phys. Earth Planet. Int.* **136** 11–24
[176] Shim S-H, Duffy T S and Shen G 2001 *Nature* **411** 571–4
[177] Chudinovskikh L and Boehler R 2001 *Nature* **411** 574–7
[178] Anderson O L, Isaak D G and Yamamoto S 1989 *J. Appl. Phys.* **65** 1534–43
[179] Jamieson J C, Fritz J N and Manghnani M H 1982 *High Pressure Research in Geophysics* ed S Akimoto and M H Manghnani (Tokyo: Center for Academic Publications) pp 27–47
[180] Heinz D L and Jeanloz R 1984 *J. Appl. Phys.* **55** 885–93
[181] Speziale S, Zha C S, Duffy T S, Hemley R J and Mao H-k 2001 *J. Geophys. Res.* **106** 515–28
[182] Holmes N C, Moriarity J A, Gathers G R and Nellis W J 1989 *J. Appl. Phys.* **66** 2962–7
[183] Fei Y, Van Orman J, Li J, van Westrenen W, Sanloup C, Minarik W, Hirose K, Komabayashi T, Walter M and Funakoshi K 2004 *J. Geophys. Res.* **109** B02305
[184] Shim S-H, Duffy T S and Kenichi T 2002 *Earth Planet. Sci. Lett.* **203** 729–39
[185] Akaogi M and Ito E 1993 *Geophys. Res. Lett.* **20** 1839–42
[186] Gu Y J, Dziewonski A M and Ekstrom G 2003 *Geophys. J. Int.* **154** 559–83
[187] Flanagan M P and Shearer P M 1998 *J. Geophys. Res.* **103** 2673–92
[188] Ono S, Katsura T, Ito E, Kanzaki M, Yoneda A, Walter M J, Urakawa S, Utsumi W and Funakoshi K 2001 *Geophys. Res. Lett.* **28** 835–8

[189] Kuroda K, Irifune T, Inoue T, Nishiyama N, Miyashita M, Funakoshi K and Utsumi W 2000 *Phys. Chem. Mineral.* **27** 523–32
[190] Nishiyama N, Irifune T, Inoue T, Ando J and Funakoshi K 2004 *Phys. Earth Planet. Int.* **143–144** 185–99
[191] Morishima H, Kato T, Suto M, Ohtani E, Urakawa S, Utsumi W, Shimomura O and Kikegawa T 1994 *Science* **265** 1202–3
[192] Matsui M, Parker S C and Leslie M 2000 *Am. Mineral.* **85** 312–6
[193] Matsui M and Nishiyama N 2002 *Geophys. Res. Lett.* **29** 1368
[194] Jackson I and Rigden S M 1998 *The Earth's Mantle: Composition, Structure and Evolution* ed I Jackson (Cambridge: Cambridge University Press) pp 405–60
[195] Akaogi M, Ito E and Navrotsky A 1989 *J. Geophys. Res.* **94** 15671–85
[196] Katsura T and Ito E 1989 *J. Geophys. Res.* **94** 15663–70
[197] Suzuki A, Ohtani E, Morishima H, Kubo T, Kanbe Y, Kondo T, Okada T, Terasaki H, Kato T and Kikegawa T 2000 *Geophys. Res. Lett.* **27** 803–6
[198] Irifune T and Isshiki M 1998 *Nature* **392** 702–5
[199] Frost D J 2003 *Earth Planet. Sci. Lett.* **216** 313–28
[200] Benz H M and Vidale J E 1993 *Nature* **365** 147–50
[201] Shearer P M and Masters T G 1992 *Nature* **355** 791–6
[202] Irifune T and Ringwood A E 1993 *Earth Planet. Sci. Lett.* **117** 101–10
[203] Karato S 1997 *Phys. Earth Planet. Int.* **99** 103–11
[204] Ringwood A E 1991 *Geochim. Cosmochim. Acta* **55** 2083–110
[205] Hirose K, Fei Y W, Ma Y Z and Mao H K 1999 *Nature* **397** 53–6
[206] Litasov K, Ohtani E, Suzuki A, Kawazoe T and Funakoshi K 2004 *Geophys. Res. Lett.* **31** L24607
[207] Kubo T, Ohtani E, Kondo T, Kato T, Toma M, Hosoya T, Sano A, Kikegawa T and Nagase T 2002 *Nature* **420** 803–6
[208] Meade C and Jeanloz R 1990 *Nature* **348** 533–5
[209] Kinsland G L 1977 *J. Appl. Phys.* **48** 978
[210] Singh A K, Mao H-k, Shu J and Hemley R J 1998 *Phys. Rev. Lett.* **80** 2157–60
[211] Duffy T S, Shen G, Shu J F, Mao H-k, Hemley R J and Singh A K 1999 *J. Appl. Phys.* **86** 6729–36
[212] Christensen N E, Ruoff A L and Rodriguez C O 1995 *Phys. Rev.* B **52** 9121–4
[213] Weidner D J, Li L, Davis M and Chen J H 2004 *Geophys. Res. Lett.* **31** L06621
[214] Weidner D J, Wang Y B and Vaughan M T 1994 *Geophys. Res. Lett.* **21** 753–6
[215] Chen J H, Weidner D J and Vaughan M T 2002 *Nature* **419** 824–6
[216] Yamazaki D and Karato S 2001 *Rev. Sci. Instrum.* **72** 4207–11
[217] Wang Y B, Durham W B, Getting I C and Weidner D J 2003 *Rev. Sci. Instrum.* **74** 3002–11
[218] Uchida T, Wang Y B, Rivers M L and Sutton S R 2004 *Earth Planet. Sci. Lett.* **226** 117–26
[219] Nishiyama N, Wang Y, Uchida T, Irifune T, Rivers M L and Sutton S R 2005 *Geophys. Res. Lett.* **32** L022141
[220] Kavner A and Duffy T S 2001 *Geophys. Res. Lett.* **28** 2691–4
[221] O'Neill B and Jeanloz R 1990 *Geophys. Res. Lett.* **17** 1477–80
[222] Kesson S E, Fitz Gerald J D and Shelley J M 1998 *Nature* **393** 252–5
[223] Lee K K M, O'Neill B, Panero W R, Shim S H, Benedetti L R and Jeanloz R 2004 *Earth Planet. Sci. Lett.* **223** 381–93
[224] Ono S, Ohishi Y, Isshiki M and Watanuki T 2005 *J. Geophys. Res.* **110** B02208
[225] Funamori N, Jeanloz R, Miyajima N and Fujino K 2000 *J. Geophys. Res.* **105** 26037–43
[226] Morishima H, Ohtani E, Kato T, Shimomura O and Kikegawa T 1994 *Geophys. Res. Lett.* **21** 899–902
[227] Mao H K, Hemley R J, Fei Y, Shu J F, Chen L C, Jephcoat A P, Wu Y and Bassett W A 1991 *J. Geophys. Res.* **96** 8069–79
[228] Funamori N, Yagi T, Utsumi W, Kondo T, Uchida T and Funamori M 1996 *J. Geophys. Res.* **101** 8257–69
[229] Fiquet G, Andrault D, Dewaele A, Charpin T, Kunz M and Hausermann D 1998 *Phys. Earth Planet. Int.* **105** 21–31
[230] Fiquet G, Dewaele A, Andrault D, Kunz M and Bihan T L 2000 *Geophys. Res. Lett.* **27** 21–4
[231] Shim S-H, Duffy T S and Shen G 2001 *Science* **293** 2437–40
[232] Serghiou G, Zerr A and Boehler R 1998 *Science* **280** 2093–5
[233] Saxena S K, Dubrovinsky L S, Lazor P and Hu J Z 1998 *Eur. J. Mineral.* **10** 1275–81
[234] Saxena S K, Dubrovinsky L S, Lazor P, Cerenius Y, Haggkvist P, Hanfland M and Hu J Z 1996 *Science* **274** 1357–9
[235] Zhang J Z and Weidner D J 1999 *Science* **284** 782–4
[236] Andrault D, Bolfan-Casanova N and Guignot N 2001 *Earth Planet. Sci. Lett.* **193** 501–8
[237] Daniel I, Cardon H, Fiquet G, Guyot F and Mezouar M 2001 *Geophys. Res. Lett.* **28** 3789–92

[238] Daniel I, Bass J D, Fiquet G, Cardon H, Zhang J Z and Hanfland M 2004 *Geophys. Res. Lett.* **31** L15608
[239] Walter M J, Kubo A, Yoshino T, Brodholt J, Koga K T and Ohishi Y 2004 *Earth Planet. Sci. Lett.* **222** 501–16
[240] Yagi T, Okabe K, Nishiyama N, Kubo A and Kikegawa T 2004 *Phys. Earth Planet. Int.* **143–144** 81–91
[241] Kubo A, Yagi T, Ono S and Akaogi M 2000 *Proc. Japan Acad. Ser.* B **76** 103–7
[242] Jackson J M, Zhang J Z and Bass J D 2004 *Geophys. Res. Lett.* **31** L10614
[243] Mao H K, Shen G and Hemley R J 1997 *Science* **278** 2098–100
[244] Andrault D 2001 *J. Geophys. Res.* **106** 2079–87
[245] Kesson S E, O'Neill H S and Shelley J M G 2002 *Phys. Earth Planet. Int.* **131** 295–310
[246] Murakami M, Hirose K, Sata N and Ohishi Y 2005 *Geophys. Res. Lett.* L03304
[247] Mao H K, Chen L C, Hemley R J, Jephcoat A P, Wu Y and Bassett W A 1989 *J. Geophys. Res.* **94** 17889–94
[248] Tarrida M and Richet P 1989 *Geophys. Res. Lett.* **16** 1351–4
[249] Wang Y B and Weidner D J 1994 *Geophys. Res. Lett.* **21** 895–8
[250] Wang Y B, Weidner D J and Guyot F 1996 *J. Geophys. Res.* **101** 661–72
[251] Shim S-H, Duffy T S and Shen G 2000 *Phys. Earth Planet. Int.* **120** 327–38
[252] Akber-Knutson S, Bukowinski M S T and Matas J 2002 *Geophys. Res. Lett.* **29** 1034
[253] Magyari-Kope B, Vitos L, Grimvall G, Johansson B and Kollar J 2002 *Phys. Rev.* B **65** 193107
[254] Stixrude L, Cohen R E, Yu R C and Krakauer H 1996 *Am. Mineral.* **81** 1293–6
[255] Kurashina T, Hirose K, Ono S, Sata N and Ohishi Y 2004 *Phys. Earth Planet. Int.* **145** 67–74
[256] Ono S, Ohishi Y and Mibe K 2004 *Am. Mineral.* **89** 1480–5
[257] Dewaele A, Fiquet G, Andrault D and Hausermann D 2000 *J. Geophys. Res.* **105** 2869–77
[258] Mao H K, Shu J, Fei Y, Hu J and Hemley R J 1996 *Phys. Earth Planet. Int.* **96** 135–45
[259] Fei Y and Mao H K 1994 *Science* **266** 1678–80
[260] Murakami M, Hirose K, Ono S, Tsuchiya T, Isshiki M and Watanuki T 2004 *Phys. Earth Planet. Int.* **146** 273–82
[261] Kondo T, Ohtani E, Hirao N, Yagi T and Kikegawa T 2004 *Phys. Earth Planet. Int.* **143–144** 201–13
[262] Mao W, Shu J F, Hu J Z, Hemley R and Mao H 2002 *J. Phys.: Condens. Matter* **14** 11349–54
[263] Dubrovinsky L S, Dubrovinskaia N A, Saxena S K, Annersten H, Halenius E, Harryson H, Tutti F, Rekhi S and Le Bihan T 2000 *Science* **289** 430–2
[264] Dubrovinsky L, Dubrovinskaia N, Annersten H, Halenius E and Harryson H 2001 *Eur. J. Mineral.* **13** 857–61
[265] Lin J F, Heinz D L, Mao H K, Hemley R J, Devine J M, Li J and Shen G Y 2003 *Proc. Natl Acad. Sci.* **100** 4405–8
[266] Kingma K J, Cohen R E, Hemley R J and Mao H K 1995 *Nature* **374** 243–5
[267] Andrault D, Fiquet G, Guyot F and Hanfland M 1998 *Science* **282** 720–4
[268] Teter D M, Hemley R J, Kresse G and Hafner J 1998 *Phys. Rev. Lett.* **80** 2145–8
[269] Leger J M and Haines J 1997 *Eur. J. Solid State Inorg. Chem.* **34** 785–96
[270] Ono S, Hirose K, Nishiyama N and Isshiki M 2002 *Am. Mineral.* **87** 99–102
[271] Ono S, Tsuchiya T, Hirose K and Ohishi Y 2003 *Phys. Rev.* B **68** 014103
[272] Prakapenka V B, Shen G Y, Dubrovinsky L S, Rivers M L and Sutton S R 2004 *J. Phys. Chem. Solids* **65** 1537–45
[273] Tsuchida Y and Yagi T 1989 *Nature* **340** 217–20
[274] Andrault D, Angel R J, Mosenfelder J L and Le Bihan T 2003 *Am. Mineral.* **88** 301–7
[275] Shieh S R, Duffy T S and Shen G 2005 *Earth Planet. Sci. Lett.* **235** 273–82
[276] Murakami M, Hirose K, Ono S and Ohishi Y 2003 *Geophys. Res. Lett.* **30** 1207
[277] Dubrovinsky L S, Saxena S K, Lazor P, Ahuja R, Eriksson O, Wills J M and Johansson B 1997 *Nature* **388** 362–5
[278] Dubrovinsky L S, Dubrovinskaia N A, Saxena S K, Tutti F, Rekhi S, Bihan T L, Shen G and Hu J 2001 *Chem. Phys. Lett.* **333** 264–70
[279] Luo S N, Tschauner O, Asimow P D and Ahrens T J 2004 *Am. Mineral.* **89** 454–61
[280] Dubrovinsky L S, Dubrovinskaia N A, Prakapenka V, Seifert F, Langenhorst F, Dmitriev V, Weber H P and Le Bihan T 2004 *Phys. Earth Planet. Int.* **143–144** 231–40
[281] Murakami M, Hirose K, Kawamura K, Sata N and Ohishi Y 2004 *Science* **304** 855–8
[282] Oganov A R and Ono S 2004 *Nature* **430** 445–8
[283] Tsuchiya T, Tsuchiya J, Umemoto K and Wentzcovitch R A 2004 *Earth Planet. Sci. Lett.* **224** 241–8
[284] Shim S-H, Duffy T S, Jeanloz R and Shen G 2004 *Geophys. Res. Lett.* **31** L10603
[285] Iitaka T, Hirose K, Kawamura K and Murakami M 2004 *Nature* **430** 442–5
[286] Shieh S R, Duffy T S, Kubo A, Shen G, Prakapenka V B, Sata N, Hirose K and Ohishi Y 2005 *EOS Trans. AGU* MR23A–0181

[287] Mao W L, Shen G Y, Prakapenka V B, Meng Y, Campbell A J, Heinz D L, Shu J F, Hemley R J and Mao H K 2004 *Proc. Natl Acad. Sci.* **101** 15867–9
[288] Hirose K, Kawamura K, Ohishi Y, Tateno S and Sata N 2005 *Am. Mineral.* **90** 262–5
[289] Kubo A, Duffy T S, Shieh S R, Kiefer B, Prakapenka V B and Shen G 2004 *EOS Trans AGU* (Fall Meeting Suppl.) MR23A–0181
[290] Stevenson D J 2003 *Earth Planet. Sci. Lett.* **208** 1–11
[291] Kivelson M G, Khurana K K, Russell C T, Walker R J, Warnecke J, Coroniti F V, Polanskey C, Southwood D J and Schubert G 1996 *Nature* **384** 537–41
[292] Saxena S K, Dubrovinsky L S, Haggkvist P, Cerenius Y, Shen G and Mao H K 1995 *Science* **269** 1703–4
[293] Dubrovinsky L S, Saxena S K and Lazor P 1998 *Eur. J. Mineral.* **10** 43–7
[294] Yoo C S, Soderlind P, Moriarty J A and Cambell A J 1996 *Phys. Lett.* A **214** 65–70
[295] Andrault D, Fiquet G, Kunz M, Visocekas F and Hausermann D 1997 *Science* **278** 831–4
[296] Andrault D, Fiquet G, Charpin T and le Bihan T 2000 *Am. Mineral.* **85** 364–71
[297] Funamori N, Yagi T and Uchida T 1996 *Geophys. Res. Lett.* **23** 953–6
[298] Ma Y Z, Somayazulu M, Shen G Y, Mao H K, Shu J F and Hemley R J 2004 *Phys. Earth Planet. Int.* **143–144** 455–67
[299] Uchida T, Wang Y B, Rivers M L and Sutton S R 2001 *J. Geophys. Res.* **106** 21799–810
[300] Brown J M and McQueen R G 1996 *J. Geophys. Res.* **91** 7485–94
[301] Vocadlo L, Alfe D, Gillan M J, Wood I G, Brodholt J P and Price G D 2003 *Nature* **424** 536–9
[302] Lin J F, Heinz D L, Campbell A J, Devine J M and Shen G Y 2002 *Science* **295** 313–15
[303] Duffy T S and Ahrens T J 1997 *J. Appl. Phys.* **82** 4259–69
[304] Duffy T S and Ahrens T J 1992 *High-Pressure Research in Mineral Physics: Applications to Earth and Planetary Sciences* ed Y Syono and M H Manghnani (Tokyo: Terra Scientific) pp 353–62
[305] Tromp J 2001 *Ann. Rev. Earth Planet. Sci.* **29** 47–69
[306] Steinle-Neumann G, Stixrude L, Cohen R E and Gulseren O 2001 *Nature* **413** 57–60
[307] Steinle-Neumann G, Stixrude L and Cohen R E 1999 *Phys. Rev.* B **60** 791–9
[308] Wenk H R, Matthies S, Hemley R J, Mao H K and Shu J 2000 *Nature* **405** 1044–7
[309] Merkel S, Wenk H R, Gillet P, Mao H K and Hemley R J 2004 *Phys. Earth Planet. Int.* **145** 239–51
[310] Antonangeli D, Krisch M, Fiquet G, Farber D L, Aracne C M, Badro J, Occelli F and Requardt H 2005 *Phys. Rev. Lett.* **93** 215505
[311] Poirier J P 1994 *Phys. Earth Planet. Int.* **85** 319–37
[312] Fei Y, Prewitt C T, Mao H K and Bertka C M 1995 *Science* **268** 1892–4
[313] Kusaba K, Syono Y, Kikegawa T and Shimomura O 1998 *J. Phys. Chem. Solids* **59** 945–50
[314] Kusaba K, Syono Y, Kikegawa T and Shimomura O 1997 *J. Phys. Chem. Solids* **58** 241–6
[315] Urakawa S, Someya K, Terasaki H, Katsura T, Yokoshi S, Funakoshi K I, Utsumi W, Katayama Y, Sueda Y I and Irifune T 2004 *Phys. Earth Planet. Int.* **143–144** 469–79
[316] King H E and Prewitt C T 1982 *Acta Crystallogr.* B—*Struct. Sci.* **38** 1877–87
[317] Nelmes R J, McMahon M I, Belmonte S A and Parise J B 1999 *Phys. Rev.* B **59** 9048–52
[318] Kobayashi H, Kamimura T, Alfe D, Sturhahn W, Zhao J Y and Alp E E 2004 *Phys. Rev. Lett.* **93** 195503
[319] Kobayashi H, Takeshita N, Mori N, Takahashi H and Kamimura T 2001 *Phys. Rev.* B **63** 115203
[320] Takele S and Hearne G R 1999 *Phys. Rev.* B **60** 4401–3
[321] Kobayashi H, Sato M, Kamimura T, Sakai M, Onodera H, Kuroda N and Yamaguchi Y 1997 *J. Phys.: Condens. Matter* **9** 515–27
[322] Fei Y W, Li J, Bertka C M and Prewitt C T 2000 *Am. Mineral.* **85** 1830–33
[323] Fei Y W, Bertka C M and Finger L W 1997 *Science* **275** 1621–3
[324] Williams Q, Jeanloz R, Bass J, Svendsen B and Ahrens T J 1987 *Science* **236** 181–2
[325] Boehler R 1993 *Nature* **363** 534–6
[326] Alfe D, Gillan M J and Price G D 1999 *Nature* **401** 462–4
[327] Alfe D, Price G D and Gillan M J 2002 *Phys. Rev.* B **65** 165118
[328] Alfe D, Vocadlo L, Price G D and Gillan M J 2004 *J. Phys.: Condens. Matter* **16** S973–S982
[329] Belonoshko A B, Ahuja R and Johansson B 2000 *Phys. Rev. Lett.* **84** 3638–41
[330] Laio A, Bernard S, Chiarotti G L, Scandolo S and Tosatti E 2000 *Science* **287** 1027–30
[331] Yoo C S, Holmes N C, Ross M, Webb D J and Pike C 1993 *Phys. Rev. Lett.* **70** 3931–4
[332] Koenig M *et al* 2004 *Nucl. Fusion* **44** S208–14
[333] Luo S N and Ahrens T J 2003 *Appl. Phys. Lett.* **82** 1836–8
[334] Nguyen J H and Holmes N C 2004 *Nature* **427** 339–42
[335] Ahrens T J, Holland K G and Chen G Q 2002 *Geophys. Res. Lett.* **29** 1150

[336] Sanloup C, Fiquet G, Gregoryanz E, Morard G and Mezouar M 2004 *Geophys. Res. Lett.* **31** L07604
[337] Sanloup C, Guyot F, Gillet P, Fiquet G, Mezouar M and Martinez I 2000 *Geophys. Res. Lett.* **27** 811–4
[338] Balog P S, Secco R A, Rubie D C and Frost D J 2003 *J. Geophys. Res.* **108** 2124
[339] Dobson D P, Crichton W A, Vocadlo L, Jones A P, Wang Y B, Uchida T, Rivers M, Sutton S and Brodholt J P 2000 *Am. Mineral.* **85** 1838–42
[340] Rutter M D, Secco R A, Uchida T, Liu H J, Wang Y B, Rivers M L and Sutton S R 2002 *Geophys. Res. Lett.* **29** 1217
[341] Terasaki H, Kato T, Urakawa S, Funakoshi K, Suzuki A, Okada T, Maeda M, Sato J, Kubo T and Kasai S 2001 *Earth Planet. Sci. Lett.* **190** 93–101
[342] Urakawa S, Terasaki H, Funakoshi K, Kato T and Suzuki A 2001 *Am. Mineral.* **86** 578–82
[343] Terasaki H, Kato T, Urakawa S, Funakoshi K, Sato K, Suzuki A and Okada T 2002 *Geophys. Res. Lett.* **29** 1227
[344] Sanloup C, Guyot F, Gillet P, Fiquet G, Hemley R J, Mezouar M and Martinez I 2000 *Europhys. Lett.* **52** 151–7
[345] Alfe D, Kresse G and Gillan M J 2000 *Phys. Rev.* B **61** 132–42
[346] Sanloup C, Guyot F, Gillet P and Fei Y 2002 *J. Geophys. Res.* **107** 2272
[347] Lin J F, Santoro M, Struzhkin V V, Mao H K and Hemley R J 2004 *Rev. Sci. Instrum.* **75** 3302–6
[348] Mao W L, Mao H K, Yan C S, Shu J F, Hu J Z and Hemley R J 2003 *Appl. Phys. Lett.* **83** 5190–2
[349] Weir S T, Akella J, Aracne-Ruddle C, Vohra Y K and Catledge S A 2000 *Appl. Phys. Lett.* **77** 3400–2
[350] Xu J A, Mao H K, Hemley R J and Hines E 2004 *Rev. Sci. Instrum.* **75** 1034–8
[351] Ito E, Katsura T, Aizawa Y, Kawabe K, Yokoshi S, Kubo A, Nozawa A and Funakoshi K 2005 *Advances in High Pressure Technology for Geophysical Applications* ed J Chen *et al* (Amsterdam: Elseveir)
[352] Akaogi M 2000 *Science* **287** 1602–3
[353] Schubert G, Turcotte D L and Olson P 2001 *Mantle Convection in the Earth and Planets* (Cambridge: Cambridge University Press) p 940
[354] Shim S-H 2005 *Structure, Composition and Evolution of the Earth's Mantle* ed R van der Hilst *et al* (Washington: American Geophysical Union) at press
[355] Uchida T, Funamori N, Ohtani T and Yagi T 1996 *High Pressure Sci. Technol.* ed W Trzeciakowski (Singapore: World Scientific) pp 183–5
[356] Meade C and Jeanloz R 1990 *Nature* **348** 533–5
[357] Merkel S, Wenk H R, Badro J, Montagnac G, Gillet P, Mao H-k and Hemley R J 2003 *Earth Planet. Sci. Lett.* **209** 351–60
[358] Dubrovinsky L S, Dubrovinskaia N A, Saxena S K, Rekhi S and LeBihan T 2000 *J. Alloys Compounds* **297** 156–61
[359] Mao H K, Shu J F, Shen G Y, Hemley R J, Li B S and Singh A K 1999 *Nature* **399** 280